Proučavanje plina neutralnog vodika u dalekim galaksijama koristeći metodu slaganja spektara

Ceraj, Lana

SVEUČILIŠTE U ZAGREBU
PRIRODOSLOVNO-MATEMATIČKI FAKULTET
FIZIČKI ODSJEK

Lana Ceraj

PROUČAVANJE PLINA NEUTRALNOG VODIKA U DALEKIM GALAKSIJAMA KORISTEĆI METODU SLAGANJA SPEKTARA

Diplomski rad

Zagreb, 2015.

SVEUČILIŠTE U ZAGREBU
PRIRODOSLOVNO-MATEMATIČKI FAKULTET
FIZIČKI ODSJEK

SMJER: ISTRAŽIVAČKI

Lana Ceraj

Diplomski rad

Proučavanje plina neutralnog vodika u dalekim galaksijama koristeći metodu slaganja spektara

Voditelj diplomskog rada: doc.dr.sc. Vernesa Smolčić

Ocjena diplomskog rada: _____

Povjerenstvo: 1. _____

2. _____

3. _____

Datum polaganja: _____

Zagreb, 2015.

Acknowledgements

Firstly, I would like to express sincere gratitude to my family: my Mother and Grandmother for unconditional lifelong support throughout school and personal life. I would like to thank Krešimir for all the emotional (and technical) support he provided me throughout all our years together.

I thank Professor Mirko Planinić and Professor Maja Planinić for giving me a chance to see what it takes to be a teacher and what fun (and responsibility) it can be. A huge thanks to Professor Ana Sušac for the joyful experience of studying and teaching physics.

I would like to express my sincere gratitude to my supervisors, Assistant Professor Vernesa Smolčić and Dr. Sc. Jacinta Delhaize for their help and guidance through the last year of my studies. The biggest thanks to Jacinta for all of the patience, kindness and support she has shown me. Jacinta, thank you for sharing your knowledge and giving me a taste of what it feels like to be an astronomer.

Proučavanje plina neutralnog vodika u dalekim galaksijama koristeći metodu slaganja spektara

Sažetak

Plin neutralnog vodika (HI) smatra se građevnom jedinicom galaksija jer služi kao primarno gorivo za stvaranje zvijezda. Izravna opažanja HI emisijske linije na 21 cm ograničena su granicama osjetljivosti radio teleskopa. Kako bi nadišli ovaj problem, koristimo relativno novu metodu slaganja spektara kako bi pomaknuli granice crvenih pomaka u radio opažanjima dalje nego li je moguće ostalim opažačkim metodama.

U ovom radu predstavljena je statistička metoda slaganja HI spektara galaksija lociranih u tzv. $G09$ nebeskom polju, u rasponu crvenih pomaka $0.039 < z < 0.134$. HI opažanja smiljena su Parkes radio teleskopom (New South Wales, Australija). Položaji galaksija i crveni pomaci nalaze se u katalogu dobavljenom iz baze podataka Galaxy and Mass Assembly (GAMA) istraživanja. Slažući spektre 7049 galaksija, ekstrahirane iz Parkes podatkovne kocke, postižemo dobar omjer signala i šuma, $S/N = 11.9$. Šum pokazuje karakteristike Gaussiana, uz malo odstupanje zbog prisutnosti rezidualne radio-frekventne interferencije i emisije od snažnih izvora u podacima.

Usrednjene veličine karakteristične HI dobivamo integrirajući složene spektre u granicama $\pm 300\ \mathrm{kms}^{-1}$ od sustava mirovanja. Taj raspon odgovara iznosu najveće očekivane širine HI profila. Srednja vrijednost gustoće toka, usrednjena masa HI i usrednjeni omjer mase i luminoziteta HI su (tim redoslijedom): $\langle S \rangle = (1.07 \pm 0.09)$mJy, $\langle M_{HI} \rangle = (2.97 \pm 0.38) \times 10^9 h^{-2} M_\odot$ i $\langle M_{HI}/L_r \rangle = (1.58 \pm 0.39)\ M_\odot L_\odot^{-1}$. Pri izračunu kozmičke gustoće mase HI (Ω_{HI}) testiramo dvije formule. Kako bi u izračun uključili i efekt konfuzije, koristimo faktor konfuzije, $\mathcal{C} = 8.6$, definiran kao srednji broj galaksija koje se nalaze unutar promjera zrake Parkes teleskopa (15.5 arcmin) i koje imaju crveni pomak ± 0.002 ($\pm 300\ \mathrm{kms}^{-1}$) jedna u odnosu na drugu. Vrijednosti Ω_{HI} dobivene u rasponu crvenih pomaka $0.039 < z < 0.134$ su $\Omega_{HI} = (1.51 \pm 0.38) \times 10^{-4} h^{-1}$ i $\Omega_{HI} = (0.51 \pm 0.07) \times 10^{-4} h^{-1}$. Primjenjena korekcija konfuzije vjerojatno je rigorozna te su naši rezultati za faktor ~3 manji od vrijednosti i predviđanja iz literature. U stvarnosti je malo vjerojatno da se u proteklih ~1.67 Gyr odvijao značajan razvoj Ω_{HI}.

Studies of neutral hydrogen gas in distant galaxies using the spectral stacking technique

Abstract

Neutral hydrogen gas (HI) is the building block of galaxies as it is a primary fuel for star formation. Direct observations of the HI 21 cm emission line are restricted by the limited sensitivities of radio telescopes. To overcome this issue, we employ the relatively new technique of spectral stacking to push the redshift limits of radio observations further than otherwise possible.

This thesis presents an HI spectral stacking analysis of galaxies within the Galaxy and Mass Assembly (GAMA) 9^h field and over the redshift range $0.039 < z < 0.134$. HI data was collected with the Parkes radio telescope in New South Wales, Australia. Galaxy positions and spectroscopic redshifts are provided by the GAMA survey. By co-adding the spectra of 7049 galaxies extracted from the Parkes data cube, we obtain a strong integrated signal-to-noise ratio of $S/N = 11.9$. The rms noise behaves in a Gaussian manner, with slight deviation caused by the residual radio frequency interference and continuum source emission in the data.

We measure average HI properties by integrating stacked spectra over ± 300 kms^{-1} from rest frame, the range equivalent to the maximum expected width of the HI profile. The resulting average flux density, average HI mass and average HI mass-to-light ratio are, respectively: $\langle S \rangle = (1.07 \pm 0.09)$mJy, $\langle M_{HI} \rangle = (2.97 \pm 0.38) \times 10^9 h^{-2} M_\odot$ and $\langle M_{HI}/L_r \rangle = (1.58 \pm 0.39) M_\odot L_\odot^{-1}$. We test two different strategies in calculating the cosmic HI mass density (Ω_{HI}). To account for source confusion effect, we apply the confusion factor $\mathcal{C} = 8.6$, the estimate of the average number of galaxies within one beam width of the Parkes telescope (15.5 arcmin) with redshift ± 0.002 (± 300 kms^{-1}). Derived values over the observed redshift range are $\Omega_{HI} = (1.51 \pm 0.38) \times 10^{-4} h^{-1}$ and $\Omega_{HI} = (0.51 \pm 0.07) \times 10^{-4} h^{-1}$. The confusion correction is likely too extreme and so our results are a factor of ~ 3 smaller than other literature values and predictions. In reality, it is unlikely that there is significant evolution of Ω_{HI} over the past $z \sim 1.67$ Gyr.

Contents

1 Introduction

1.1 Thesis overview

Galaxies are complex, gravitationally bound systems of stars, interstellar gas, dust and dark matter. Their evolutionary pathways through different epochs are still greatly unknown. The aim of this thesis is to explore the cosmic evolution of neutral hydrogen gas, an essential component of galaxies, which serves as the raw fuel for the star formation. The strategy that is used in this study is the relatively new technique of spectral stacking which enables one to find average properties of HI gas within a large sample of individually undetected galaxies.

In Section 1.2 of Chapter 1 I briefly summarize the current knowledge on the evolution of galaxies and how their content changes over cosmic time. Section 1.3 provides a description of the 21cm hyperfine line of neutral atomic hydrogen (HI). The purpose of Section 1.4 is to serve as an introduction to the theoretical and observational framework of Ω_{HI} evolution and as an introduction to the stacking method.

1.2 Galaxy evolution

The study of galaxy evolution differs from most other areas of experimental physics due to the fact that even the shortest timescales involved are much longer than that of a human life. Due to the expansion of the Universe, an object that is farther away will have a larger receding velocity, and thus a higher redshift. Thanks to the finite speed of light, we are able to look at galaxies at large distances from us, which is equivalent to observing a younger Universe. By observing galaxies at different distances (i.e. different moments in their past) we can study how they form and evolved over time. Figure 1.1 shows the chart of how galaxies form. This chart is based on the current view of galaxy formation and evolution, and may change in the future [1].

Galaxies play a crucial role in the study of the structure and evolution of the Universe because of their abundance, which enables us to use them as the tracers of the evolution of the Universe as a whole. In the study of galaxy evolution over cosmological lengths and time scales, a cosmological model of the Universe has to be specified. Currently, the most popular cosmological model is referred to as ΛCDM or the standard model. It is based upon the

Cosmological Principle and Einstein's theory of General Relativity. A ΛCDM Universe is flat and contains roughly 75% dark energy, 21 % cold dark matter (CDM) and only 4% of baryonic matter. The latest measurements of cosmological parameters, presented in *Planck 2015 results. I. Overview of products and scientific results* [2], show that the Universe contains of 69.36% dark energy, 25.8% dark matter and 4.84% baryonic matter.

However, the standard model cannot explain the origin of the large scale structures that are seen today. An expansion of the standard model, which gives the solution for the so called "horizon problem", was suggested by Alan H. Guth [3] under the name "*inflation*". Inflation is assumed to be an era in which the young Universe has gone through a phase of rapid exponential expansion driven by the vacuum energy of quantum fields. The theory of inflation explains the origin of large scale structures as density perturbations which are a consequence of the quantum fluctuations in the vacuum energy of the early Universe. Density perturbations as part of the expanding Universe grow with time. Regions in which initial densities were slightly higher than the mean density attracted their surroundings stronger than average. This means that over-dense regions pulled matter towards them and became even more over-dense. On the other hand, under-dense regions became even more under-dense. This process of amplification of density perturbations is referred to as *gravitational instability* and it plays an important role in structure formation. At first, the size of over-dense regions increases with time due to the expansion of the Universe. Once a perturbation reaches some critical over-density, it starts to collapse.

In ΛCDM, each initial perturbation consists of both dark and baryonic matter. When an object collapses, the dark matter forms a dark matter halo through a process of violent relaxation. The baryonic gas shocks to the virial temperature and then, depending on the cooling process, may settle into hydrostatic equilibrium in the potential well of the dark matter halo.

Depending on the temperature and density, a variety of cooling processes can affect the gas. Cooling rates depend strongly on the chemical composition of the gas. In halos in which the virial temperature is below 10^4 K, the gas is mostly neutral. If heavy elements and molecules are present, cooling is possible through collisional excitation of fine and hyperfine structure lines for heavy elements or rotational and vibrational lines for molecules. The net effect of cooling is that the baryonic material segregates from the dark matter and accumulates as cold gas in a protogalaxy at the center of the dark matter halo. As the result of the conservation of angular momentum, the gas will settle into a disk about the center of the galaxy. As the gas

continues to cool its self-gravity will eventually dominate over the gravity of the dark matter and collapse. This collapse increases the temperature and density of the gas, which reduces the cooling time. This may cause gas clouds to fragment into smaller high density cores. If the cooling is efficient enough, gas condenses and stars begin to form (e.g. Cole et al. (2000)[4]).

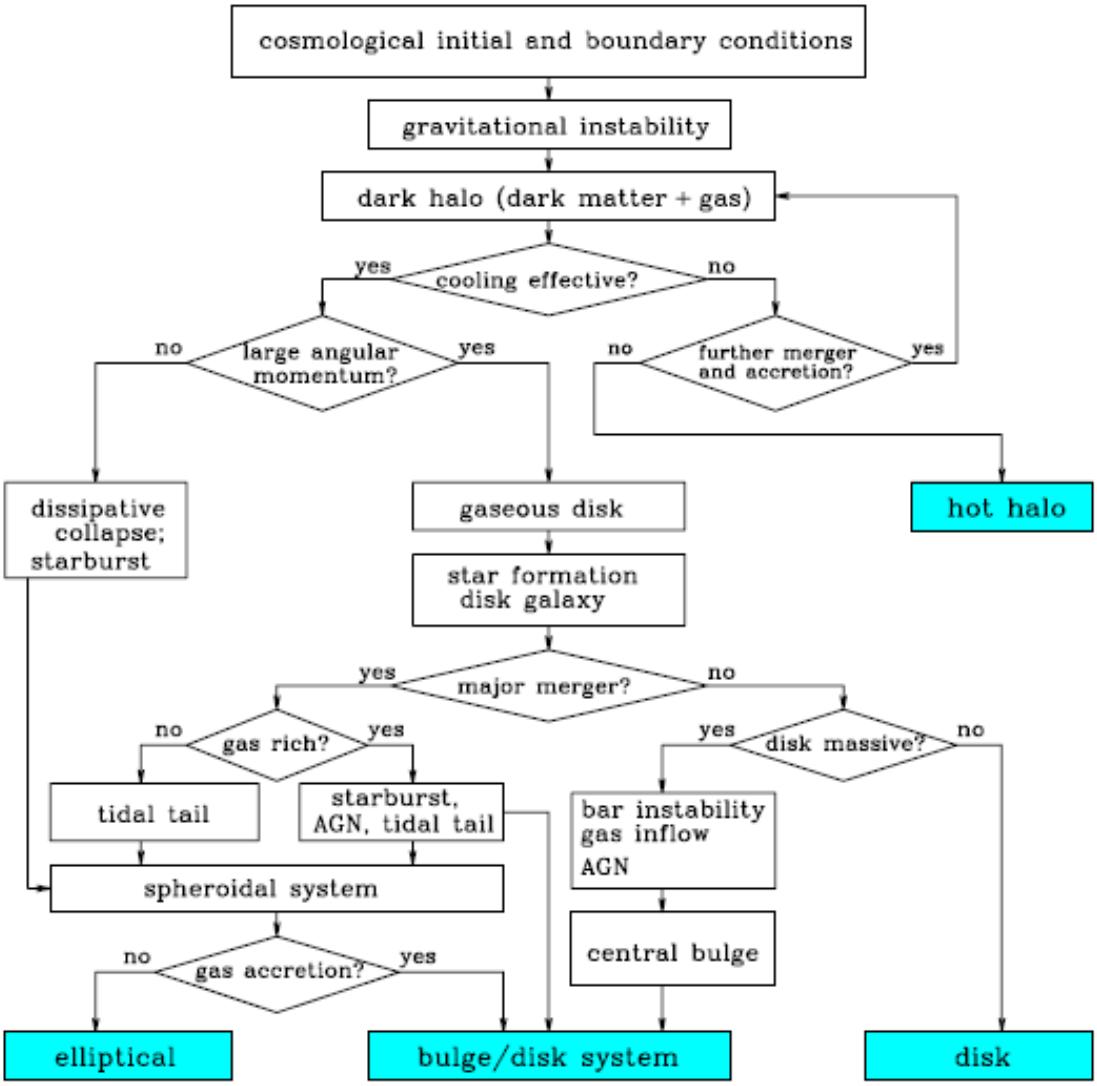

Figure 1.1: Galaxy formation chart. This chart reflects our current view of galaxy formation. Image reproduced from [1].

An important aspect to consider while studying galaxy evolution is that galaxies and dark matter halos are not isolated; they can accrete or lose material through interaction with the intergalactic medium and *feedback processes*. The feedback processes may prevent the gas from

cooling. For example, supernovae explosions release radiation and blastwaves that may heat and reheat surrounding gas, blowing it out of the galaxy. Also, material accreting onto supermassive black holes, which are presumed to be found at the centers of almost all massive galaxies, release vast amounts of energy which may reheat the cold gas (e.g. Di Matteo et al., 2005 [5]). This is referred to as an *active galactic nucleus* (AGN). Aside from the feedback processes, two or more dark matter halos can merge, which creates a larger dark matter halo. If these halos contain central galaxies, which also merge, gas can be compressed and there can be an increase in the star formation rate (SFR) [6].

Therefore, galaxies are complex, multicomponent systems whose evolution is affected by the abundance of every component and by the processes that drive the evolution of the dark and baryonic matter within them. In order to gain a full understanding of a galaxy's evolutionary pathway, we need to examine it at all wavelengths, from infrared to ultraviolet and carefully study the various physical processes.

1.3 Neutral hydrogen gas

An essential component that is most likely to play an important role in the evolution of galaxies is cold ($< 10^4$ K) hydrogen gas. Hydrogen is the most abundant element in the Universe. It can be found in galaxies as neutral hydrogen (HI), ionised hydrogen (HII) and as molecular hydrogen (H_2). This thesis will primarily focus on neutral hydrogen, hereafter referred to as "HI". It can be detected via its hyperfine emission line of wavelength 21.105 cm.

The proton and the electron in the hydrogen atom constitute tiny magnetic dipoles whose interaction energy depends on the relative orientations of their spins [7]. In the parallel state, the energy is higher than in the antiparallel state. The difference in the energy of two states is $5.87 \cdot 10^{-6}$ eV. When a spontaneous spin-flip occurs from the state of higher to the state of lower energy, a photon of frequency 1420.406 MHz and of wavelength 21.105 cm is emitted. This transition is forbidden and the lifetime in the excited state is $1.1 \cdot 10^7$ years. However, the lifetime is significantly shortened in gas clouds due to collisions between atoms, making the transition more frequent and making it possible to detect the presence of HI via the 21cm emission line.

It is possible for us to derive the HI mass of a galaxy directly from the observed $21\ cm$ flux density spectrum if we assume the Rayleigh-Jeans low frequency limit and an optically thin medium via:

$$M_{HI} = \frac{16\pi m_H}{3h\nu_0 A} D_L^2 \int S(\nu) d\nu, \tag{1.1}$$

where m_H is the mass of the hydrogen atom, h is Planck's constant, ν_0 is the frequency of the HI transition at rest frame ($\nu_0 = 1420.406$ MHz), A is Einstein's coefficient for spontaneous emission, D_L is the luminosity distance to the galaxy and $S(\nu)$ is the observed flux density.

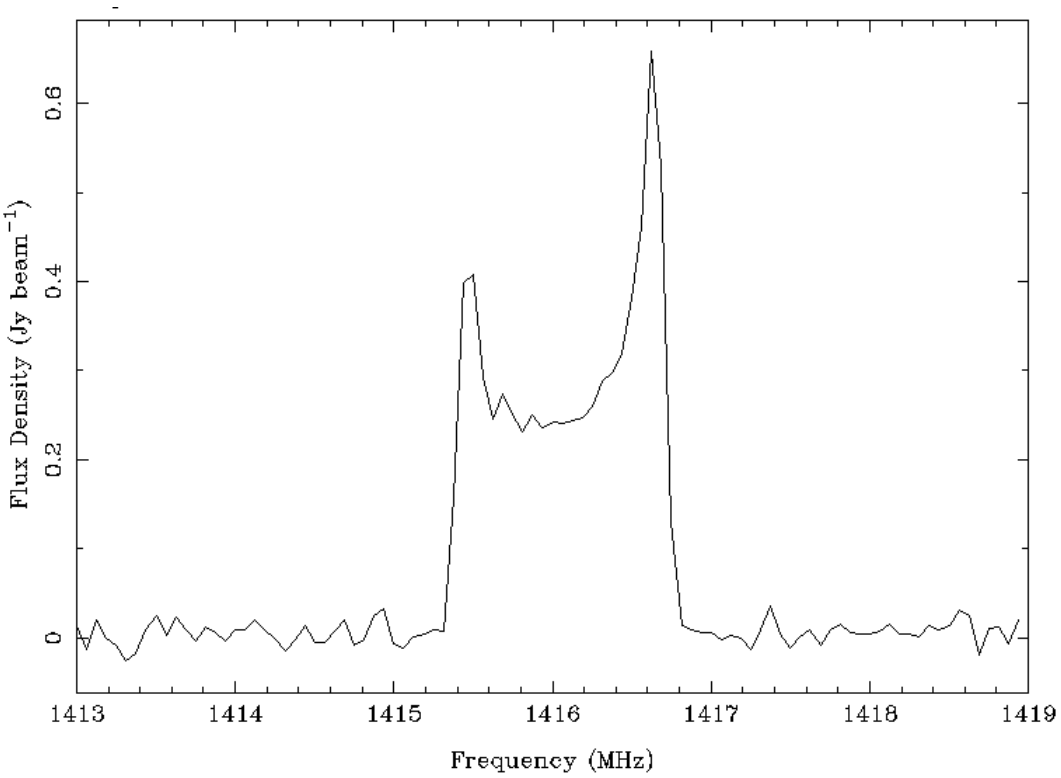

Figure 1.2: The double-horned HI profile of a typical spiral galaxy HIPASSJ0547-34. Available via the HIPASS online archive at http://www.atnf.csiro.au/research/multibeam/release/ [8],[9],[10].

The shape of the observed HI profile depends on the kinematics within the observed galaxies [11]. The characteristic double-horned profile, such as that shown in Figure 1.2, is the result of the ordered rotation of HI gas within a spiral galaxy. Single-peak profiles may occur as the result of the observer's angle of inclination or in irregular galaxies due to the random motion of gas [12].

Neutral hydrogen gas is important in astrophysics because it serves as a reservoir of fuel for future star formation. Tracing the amount of HI gas at different redshifts may help us to

explain the variation in star formation rates of galaxies over cosmic time. Figure 1.3 shows the evolution of the cosmic density of HI with redshift compared to the observed evolution of the cosmic star formation rate density (Hopkins & Beacom, 2006) [13] and the corresponding build-up of stellar mass (Wilkins et al., 2008) [14]. Data plotted in this figure will be discussed in the next section.

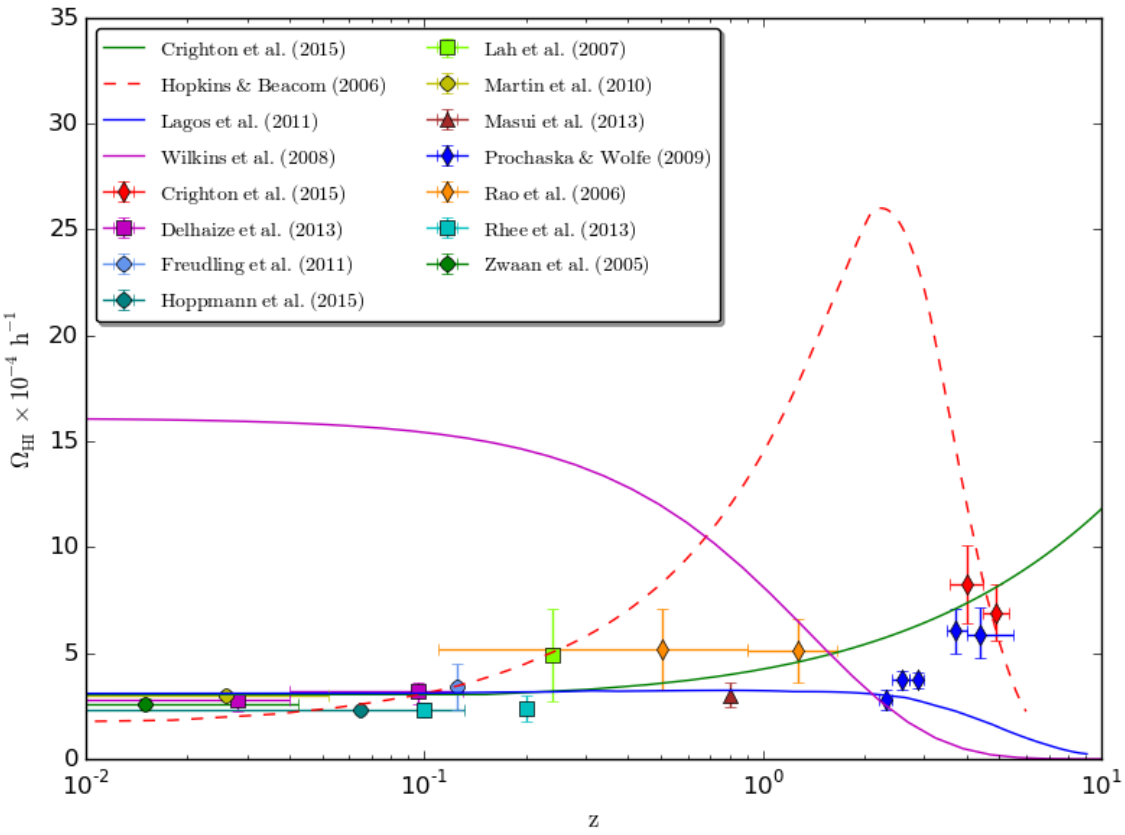

Figure 1.3: The evolution of the cosmic HI mass density, Ω_{HI}. Observational measurements are shown as points. Circular points have been derived using direct $21cm$ line detection, diamonds with damped Lyman α measurements, triangles with intensity mapping methods and squares with stacking technique. The solid pink line shows the evolution of the cosmic stellar mass density [14]. The dashed red line shows the evolution of the cosmic star formation rate density scaled by the factor of $10^{9.5}$ to highlight the extent of evolution compared with that of Ω_{HI} [13]. The solid blue line shows the semi-analytical prediction of the Ω_{HI} evolution [15]. The solid green line is the power-law fitting to the literature data performed by Crighton et al. (2015) [16].

1.4 HI detection methods

There are a number of ways to trace the HI content of galaxies. In the text below I will shortly describe several methods of obtaining the information on the evolution of galaxy components, most importantly, of HI gas.

1.4.1 Simulations

In the context of tracing the HI content of galaxies, *simulations* can be used to predict evolution of the cold gas component. The two main approaches are the use of semi-analytical models or hydrodynamical simulations. Semi-analytical models use a dark matter halo merger tree framework with the implementation of a galaxy formation prescription, whereas hydrodynamical simulations directly model gas dynamics. Lagos et al. 2011 [15] studied the evolution of the cold gas content of galaxies by splitting the interstellar medium (ISM) into its atomic and molecular hydrogen components. Their semi-analytical high resolution simulation prediction of cosmic HI density evolution (as seen in Figure 1.3) agrees relatively well with $z = 0$ observations of the HI mass density ρ_{HI} and with the observed evolution inferred from damped Lyman α systems (DLAs). However, simulations in general are limited by the particular prescription of physical processes included and by the considerable processing power required to track HI gas over a wide range of space and time.

1.4.2 21cm surveys

Direct observations and measurements of the cold gas properties are possible through sky surveys conducted using telescopes stationed all around the globe. Due to limitations of currently available telescopes, one has to compromise between making wide field-of-view observation of the local Universe and making narrower high redshift observations. In the text below I will describe some of the most influential surveys of the local Universe (HIPASS and ALFALFA) and deep surveys (AUDS and CHILES) aimed at detecting the HI content of the Universe up to a redshift 0.45.

The first blind, all-sky $21\mathrm{cm}$ survey, HI Parkes All Sky Survey (HIPASS), was conducted using the Parkes 64 m telescope. HIPASS observations were carried out between 1997 and 2002 and mapped the entire sky south of Declination $+25°$ detecting 5317 galaxies

up to a redshift 0.0423. Zwaan et al. (2005) [17] used the first version of the HIPASS source catalogue (HICAT) [18] of 4315 extragalactic 21 cm emission-line detections to calculate the HI mass function (hereafter referred to as $HIMF$) of galaxies and to closely constrain the faint end of the $HIMF$. They found the precise value of Ω_{HI} in the local Universe (z~0.015) to be $(2.6 \pm 0.3) \times 10^{-4}\ h^{-1}$ (as shown in Figure 1.3).

In 2004, the seven beam receiver called ALFA (Arecibo L-band Feed Array) was commissioned on the 305 m dish of the Arecibo Observatory in Puerto Rico. The Arecibo Legacy Fast ALFA (ALFALFA) HI survey was conducted in the period 2005 – 2012. Martin et al. (2010) [19] used the 40% completed ALFALFA survey with a coverage of $2607\ \mathrm{deg}^2$ and 10119 direct detections to generate the $HIMF$ and estimated Ω_{HI} at z~0.026 to be $(3.01 \pm 0.21) \times 10^{-4}\ h^{-1}$. This is 16% higher than the result presented in [17].

The ALFA Ultra Deep Survey (AUDS) 21 cm spectral survey was conducted with the Arecibo 305 m telescope between 2008 and 2013. The pilot study for the AUDS was conducted from October 2004 to February 2005 by Freudling et al. (2011) [20]. They detected 18 21 cm emission lines in the redshift range $0.07 < z < 0.15$ from which they estimated the mean HI mass density at z~0.125 to be $(1.0 \pm 0.3)\rho_{HI}$ which can be used to calculate a cosmic HI density of $\Omega_{HI} = (3.4 \pm 1.1) \times 10^{-4} h^{-1}$. Hoppmann et al. (2015) [21] published the results of 60% of the total survey corresponding to a sensitivity level of 80 μJy. They have detected 102 galaxies in two fields of combined area of $1.35\ \mathrm{deg}^2$ and computed the $HIMF$ at the highest redshifts to date. Using the measured $HIMF$, they found the cosmic HI density of $\Omega_{HI} = (2.33 \pm 0.07) \times 10^{-4} h^{-1}$ at z~0.065.

The Karl G. Jansky Very Large Array (JVLA) in Soccoro, New Mexico, is the upgraded version of Very Large Array (VLA) whose new, improved receivers and new backend provide a large field of view, improved sensitivity and a wider instantaneous bandwidth. The Cosmological Evolution Survey (COSMOS) HI Large Extragalactic Survey (CHILES) is a blind HI survey over $0 < z < 0.45$ that is being planned to use this new advancements of JVLA. Fernández et al. [22] completed the pilot survey for CHILES in order to test its feasibility of carrying out a full HI deep field survey. They observed a $34 \times 34\ \mathrm{arcmin}^2$ subset of the COSMOS field for 50 hours over the redshift interval $0 < z < 0.193$ and detected neutral hydrogen gas in 33 galaxies in a variety of environments. It is expected that the full CHILES

survey will probe out the Universe out to a redshift 0.45 using a similar setup and observing the same target as described in Fernández et al. (2013) [22].

1.4.3 Indirect detections at high redshift

Neutral hydrogen gas at higher redshifts can be observed using damped Lyman α systems (DLAs). DLAs are a class of quasi-stellar objects (QSO) with HI column densities higher than 2×10^{20} cm^{-2}. Of all known quasi-stellar absorption systems, DLAs dominate the neutral gas content of the Universe up to the redshift ~ 5 [23] and as such serve as neutral gas reservoirs for star formation. Prochaska et al. (2005) [24] found that the density of HI gas declines by 50% between $z\sim 3.5$ and $z\sim 2.3$. By examining 738 DLAs over the redshift interval $2.2 < z < 5$ identified in Sloan Digital Sky Survey (SDSS) spectra, Prochaska & Wolfe (2009) [25] found no evidence of the evolution of HI gas over the past ~ 10 Gyr. However, they argued that there has been a period of rapid evolution, driven by violent feedback processes that removed HI gas from nearly half of the galaxies, over the ~ 2 Gyr interval centered at $z\sim 3$.

Crighton et al. (2015) [16] measured Ω_{HI} using a homogenous sample of 163 QSO spectra with redshifts $3.56 < z < 5.31$ provided by the Giant Gemini GMOS Survey (GGG Survey). Uncertainties in the identification of DLAs are a result of strong intergalactic medium absorption and QSO continuum placement, which can cause real DLAs to be missed or bias in the column density distribution. Crighton et al. corrected data for these effects thus making the most precise high-redshift measurement of the cosmological HI mass density $\Omega_{HI} = (6.86^{+1.4}_{-1.26}) \times 10^{-4} h^{-1}$. By comparing to literature measurements at lower redshifts, they show that Ω_{HI} can be described by the functional form $\Omega_{HI}(z) = 2.8 \times 10^{-4}(1+z)^{0.6}$ produced by fitting of the binned data to a simple power law. They comment that the fitting is not physically motivated, but it does describe the observations over the redshift range $0 < z < 5$.

1.4.4 Statistical detections

The methods described above for tracking the HI distribution rely either on the direct detection of the 21cm line or DLA measurements. Direct detections are limited by the technical capabilities of the current generation of telescopes, which restricts their observations to the nearby Universe. The highest redshift direct detection were obtained at $z\sim 0.2$ by Zwaan et al.

(2001) [26], Verheijen et al (2007) [27] and Catinella et al. (2008) [28]. DLA measurements are difficult to make at $z < 1.65$ where the line shifts from optical to UV part of the spectrum and cannot be observed from the Earth's surface. In order to overcome the limitations of these methods, we use another approach in the study of the evolution of HI content of galaxies by achieving a statistical detection. In the next few paragraphs I will describe the method of intensity mapping and the spectral stacking technique, the latter of which is the focus of this thesis.

The strategy of *intensity mapping* allows one to directly map the 3D structure of the Universe at high redshifts by measuring line emission with coarse resolution [29]. Emission from many galaxies is contained within an intensity map. Using this, one can study the large-scale HI distribution without the need to resolve individual galaxies. This method makes it possible to survey extremely large volumes by using the cross-correlation between optical and 21 cm data sets. Chang et al. (2010) [30] were the first to make a detection of HI in the range $0.53 < z < 1.12$ using intensity mapping. Radio spectra were recorded across two of the DEEP2 fields by the Green Bank Telescope (GBT). The cosmic HI mass density value was measured to be $\Omega_{HI} = (3.88 \pm 1.06) \times 10^{-4} h^{-1} \times \frac{1}{rb}$, where r is galaxy-hydrogen correlation coefficient and b is the bias parameter. Poor theoretical constrains of rb values, which was estimated to be in range $0.5 < rb < 2$, motivated Masui et al. (2013) [31] to perform 21 cm intensity mapping of the data acquired at the GBT and cross-correlated with large-scale structure traced by galaxies in the WiggleZ Dark Energy Survey. They found Ω_{HI} to be $(3.03 \pm 0.56) \times 10^{-4} h^{-1} \times \frac{1}{rb}$ and presented new constraints on the r and b parameters, estimating them to be in ranges $0.65 < b < 1$ and $0.9 < r < 0.95$. In order to improve the method of intensity mapping, better measurements of the bias parameter and cross-correlation coefficient are still required.

The spectral stacking technique is a relatively new method of obtaining a statistical detection of HI line emission from an ensemble of galaxies in which there may have been no previous direct detection. The technique of spectral stacking relies on two sets of data: (i) HI data over the relevant redshift range, (ii) sky positions and redshifts of known galaxies in the field. Information on sky positions and redshifts, can be provided by external catalogues of optical spectroscopic redshift surveys, such as the Sloan Digital Sky Survey (SDSS), the Two-

degree-Field Galaxy Redshift Survey (2dFGRS) and the Galaxy and Mass Assembly (GAMA) survey. The last of which is used in the data analysis in this thesis. The radio data cube contains all radio data collected by the telescope in the observed field. By using information on sky positions and redshifts, we extract spectra for each galaxy in the sample and then shift each to rest frame. By stacking these individually low signal-to-noise spectra, we retrieve a statistical detection.

This technique has recently been examined by a number of authors (e.g. Chengalur et al. (2001) [32], Lah et al. (2009)[33], Fabello et al. (2011)[34], Maddox et al. (2013)[35]) and was found to be a great tool for examining various average physical parameters of galaxies at redshifts higher then otherwise possible. Lah et al. (2007) [36] used observations from the Giant Metrewave Radio Telescope (GMRT) to study a sample of galaxies at $z = 0.24$. The Anglo – Australian Telescope (AAT) was used to obtain optical redshifts for these galaxies. They measured $\Omega_{HI} = (6.37 \pm 2.94) \times 10^{-4} h^{-1}$ which is consistent with DLA measurements. Delhaize et al. (2013) [37] stacked the data collected with the Parkes Radio Telescope. The optical redshifts were provided by 2dFGRS. They stacked two samples of galaxies, the first of which sample used Parkes observations of a $42\ \mathrm{deg}^2$ field near the South Galactic Pole (SGP) and contained 3277 2dFGRS galaxies over the redshift range $0.04 < z < 0.13$. The second sample contained 15093 2dFGRS objects in the range $0 < z < 0.04$ and was observed by the HIPASS. They found $\Omega_{HI} = (3.19^{+0.43}_{-0.59}) \times 10^{-4} h^{-1}$ for the SGP sample and $\Omega_{HI} = (2.82^{+0.30}_{-0.59}) \times 10^{-4} h^{-1}$ for the HIPASS sample. Rhee et al. (2013) used Westerbork Synthesis Radio Telescope (WSRT) to observe 21 cm emission lines at redshifts z~0.1 and z~0.2. Optical redshifts were provided by the CNOC2 redshift survey. For the sample containing 59 galaxies at z~0.1 they found $\Omega_{HI} = (2.31 \pm 0.35) \times 10^{-4} h^{-1}$. Measured Ω_{HI} for the 96 galaxies sample at z~0.2 was $\Omega_{HI} = (2.38 \pm 0.63) \times 10^{-4} h^{-1}$. Results from Delhaize et al. (2013) [37] and Rhee et al. (2013) [38] were consistent with estimates of Ω_{HI} made via direct detections in the HIPASS, ALFALFA and AUDS surveys. A more detailed description of the stacking technique will be presented in Sections 3.2 and 3.3. The summary of all results mentioned in Section 1.4 is displayed in Table 3.3.

1.5 Context of this work

The work presented in this thesis uses the spectral stacking technique to obtain the average properties of HI gas and to measure the comic HI mass density, Ω_{HI}, over the $0.039 < z < 0.134$ in order to examine it's evolution. To carry out this method, we use two sets of data: (i) the positions and high quality redshifts provided by the Galaxy and Mass Assembly (GAMA) survey and (ii) wide-field HI data observed with the Parkes radio telescope. A detailed description of these is provided in Chapter 2. High quality GAMA redshifts and the more sensitive HI Parkes radio data enables us to improve upon previous stacking studies in this redshift range. For example, the GAMA-II extends 1.5 magnitudes deeper than the 2dFGRS sample used by Delhaize et al. (2013) [37]. In Chapter 3, the stacking technique is presented and described (Sections 3.1 – 3.4). In Sections 3.5 and 3.6 I present and discuss the results obtained by the analysis. Finally, Chapter 4 summarizes the conclusions of this thesis and suggest methods for improving results.

Throughout this thesis we use ΛCDM cosmology with a reduced Hubble constant $h = H_0/(100\mathrm{kms}^{-1}\mathrm{Mpc}^{-1}) = 1.0$, $\Omega_\Lambda = 0.7$ and $\Omega_m = 0.3$.

2 The data

This thesis uses spectroscopic redshifts provided by the second Galaxy And Mass Assembly data release (GAMA-II) [39] and radio observations collected with the Parkes radio telescope. These data sets are described in detail in this chapter.

2.1 Galaxy and Mass Assembly

The Galaxy and Mass Assembly survey is one of the largest spectroscopic surveys of low-redshift galaxies with r-band magnitudes $r < 19.8$ identified in SDSS. The GAMA redshift survey has been operating since 2008 on the 3.9 m Anglo – Australian Telescope (AAT) [40] using the AAOmega spectrograph. The multiwavelength imaging data were collected using several different telescopes, all together contributing to a large GAMA database. It provides the optical source positions and high quality redshifts required for the stacking analysis. The first phase of the GAMA survey, referred to as GAMA-I, was conducted over the course of three years (2008 February – 2010 May) and covers three equatorial $48\ \mathrm{deg}^2$ fields centered at Right Ascension 9^h $(G09)$, 12^h $(G12)$ and 14.5^h $(G15)$ [41]. The second phase, GAMA-II survey, refers to the entire GAMA-I dataset and all subsequently collected data [39]. The main changes introduced in GAMA-II are the expansion of the $G09$, $G12$ and $G15$ fields by $12\ \mathrm{deg}^2$, as well as the addition of two extra regions $G02$ ($\sim 56\ \mathrm{deg}^2$) and $G23$ ($\sim 60\ \mathrm{deg}^2$). They also increased the limiting magnitude from $r < 19.4$ to $r < 19.8$ mag for the $G09$ field. The spectroscopic redshifts in GAMA-I have accuracy of $65\ \mathrm{kms}^{-1}$ [41]. Redshifts provided by the GAMA-II were re-calculated using fully automated code `AUTOZ` [42] with which they obtained redshift accuracy of $27\ \mathrm{kms}^{-1}$ [39].

This thesis uses GAMA-II data within the $G09$ field (shown in Figure 2.1). The GAMA-II survey provides a high spatial density of objects over the redshift range of interest, i.e. a large sample of galaxies available for stacking. That, along with the fact that it has very high quality redshifts and contains the least bright, contaminating continuum sources of the GAMA fields, makes it a great asset for a spectral stacking analysis. The internal GAMA data used for this thesis are the catalogue of sources and spectroscopic redshifts (SpecObjv27) [39] and the stellar mass catalogue (StellarMassesv18) [43] which contains the r-band absolute magnitudes. The SpecObjv27 catalogue, aside from the GAMA measurements, also contains spectroscopic

redshifts from 12 other surveys, including the SDSS and 2dFGRS surveys. Together, these provide a full compilation of all spectra available in the field of interest.

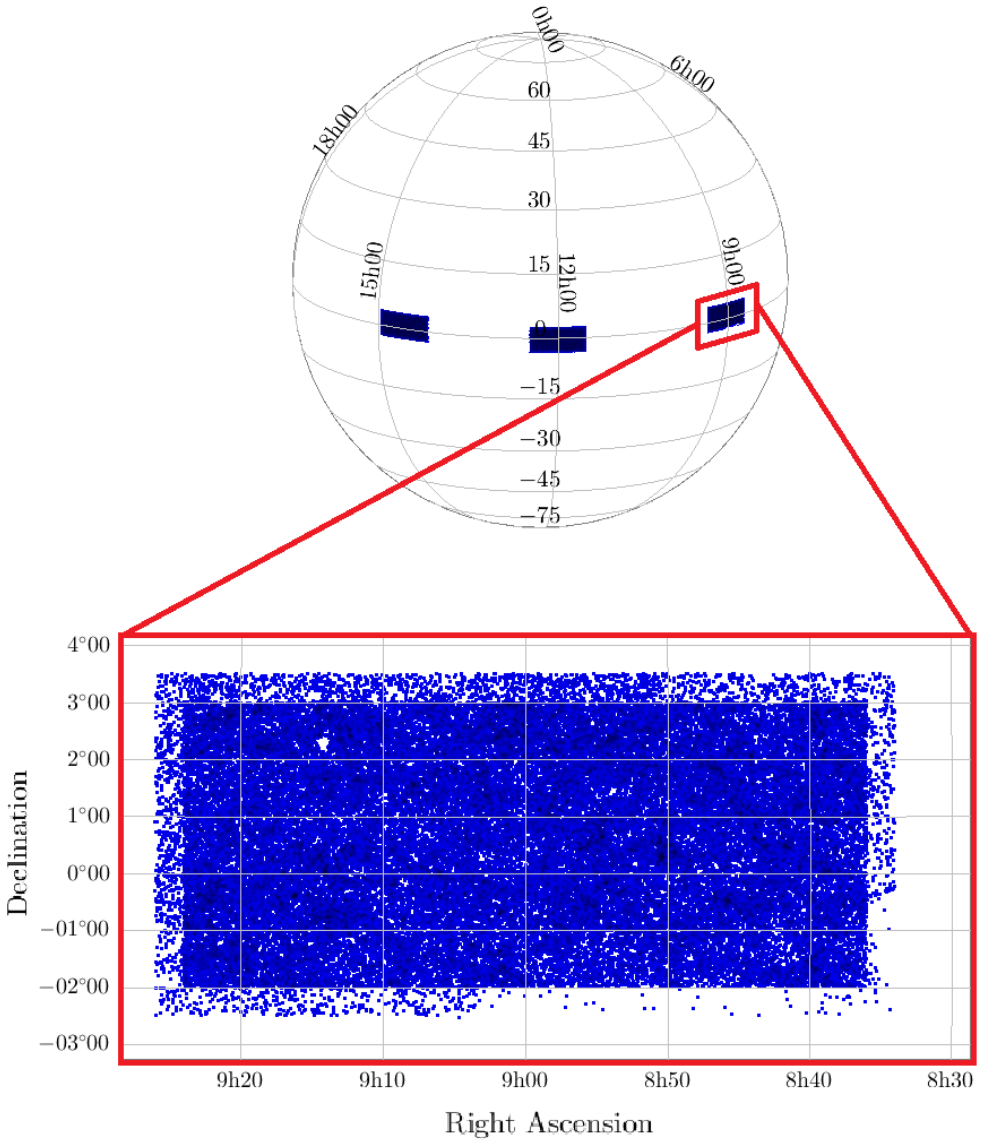

Figure 2.1: The positions of the $G09$, $G12$ and $G15$ fields from the GAMA-II catalogue of sources and spectroscopic redshifts. Enlarged is the area of the $G09$ field centered at Right Ascension 9^h which contains 75378 objects. The low density region around the edge corresponds to sources gathered from surveys other than GAMA.

2.2 Parkes observations

21 cm observations of the $G09$ field were conducted with the Parkes radio telescope located in New South Wales, Australia. The Parkes radio telescope is one of the largest single-dish telescopes in the southern hemisphere with a dish diameter of 64 m. Observations lasted over the course of two years (2010-2012) and were performed by Delhaize et al. (in prep) [44] using the multibeam receiver [45] with 104 h of on-source integration time. The observing strategy used two 64 MHz frequency bands centered on 1285 MHz and 1335 MHz with a 14 MHz band overlap to reduce the impact of the bandpass subtraction. The total frequency coverage was $1253 - 1367$ MHz with a 62.5 kHz frequency channel spacing. After data reduction, the frequency resolution was 125 kHz. Full details of the observations and data reduction can be found in Delhaize (2014) [46]. Parkes observations cover only the GAMA-I region, i.e. they miss the lower strip of the GAMA-II region ($-2° < \text{Declination} < -1°$).

A data cube, whose dimensions are Right Ascension (RA), Declination (Dec) and frequency (ν), with pixel widths 4×4 arcmin^2 was constructed for the $G09$ field and has a spatial resolution of 15.5 arcmin. Table 2.1 shows parameters of the data cube. The HI redshift associated with a particular frequency channel can be calculated using:

$$z = \frac{\nu_0}{\nu} - 1, \tag{2.1}$$

where ν is the frequency of the channel, ν_0 is the frequency of the HI transition at rest frame ($\nu_0 = 1420.406\ MHz$) and z is the corresponding redshift. The data cube has an rms noise level of 4 mJy. There were no direct HI detections.

Parameter	Interval
Right Ascension	$8^h\ 36^m - 9^h\ 24^m$
Declination	$(-1°) - (+3°)$
Frequency	$(1253 - 1367)\ MHz$
Redshift	$0.0390 - 0.1336$

Table 2.1: Parameters of the Parkes data cube.

3 Analysis and results

3.1 Source selection

We first select objects in the $G09$ field which are suitable for a stacking analysis. There are 75378 objects within the full $G09$ field. We only include galaxies in the spatial region and spectral range covered by the radio cube (see Table 2.1). Also, the 31 sources in the StellarMassesv18 catalogue for which the template fitting procedure has failed were excluded from the sample since we require magnitudes provided by this process [43]. This results in a final catalogue of 7049 sources available for stacking. Figure 3.1 shows the redshift distribution of those galaxies with the mean redshift of the sample $\langle z \rangle = 0.086$. The spatial distribution of the 7049 galaxies within $G09$ field is shown in Figure 3.2. As these two figures highlight, there appears to be some cosmic structure at redshifts $\sim 0.055, 0.07, 0.011$ which emphasize the need for a large sample of galaxies for stacking analysis to minimize the effect of cosmic variance.

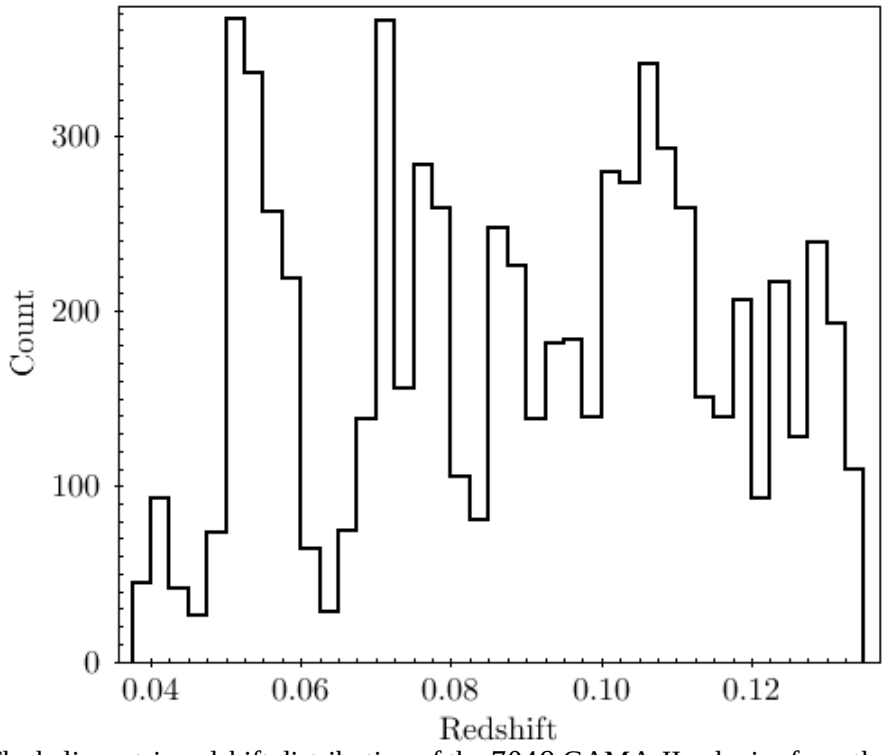

Figure 3.1: The heliocentric redshift distribution of the 7049 GAMA-II galaxies from the final catalogue used in the stacking analysis. The average redshift is 0.0860.

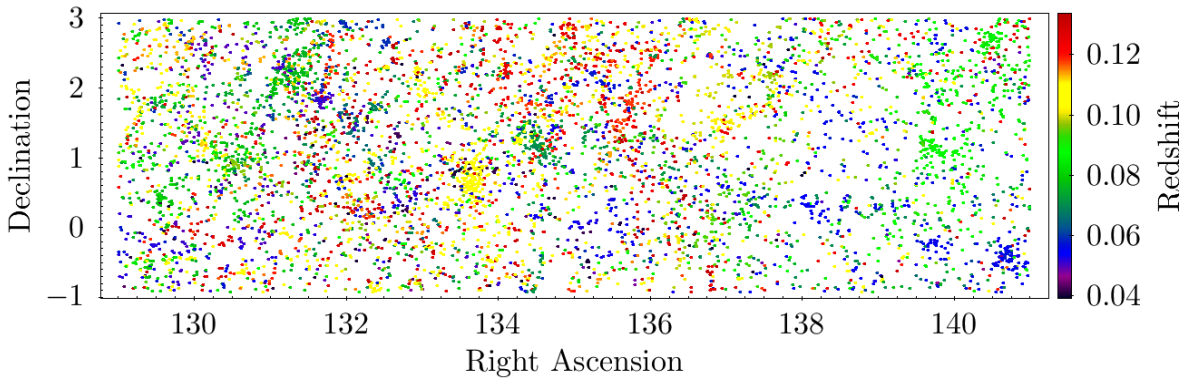

Figure 3.2: The distribution of the 7049 galaxies in the $G09$ field that are used in stacking analysis. The color scale indicates redshift.

3.2 Extraction of spectra

The *HI* data cube, as previously discussed, has RA, Dec and ν axis, but there are no direct detection of galaxies. In order to find out where the galaxies are in the data cube, we use the independent, optical source catalogue described in Section 2.1 above. As shown in Figure 3.3, the optical source catalogue provides the information on RA and Dec of each galaxy in the region covered by the radio data cube. The *HI* spectrum is extracted at this pixel position for each galaxy using the `MBSPEC` task in a radio interferometry data reduction package `MIRIAD` [47].

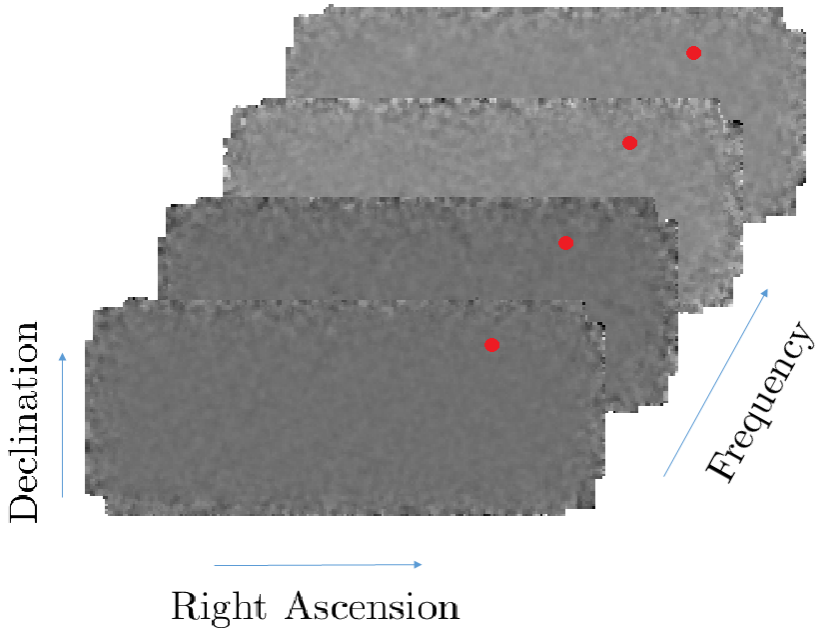

Figure 3.3: The process of extracting *HI* spectrum from the radio data cube. The red dot shows the position of a galaxy within data cube, identified in optical catalogue, at which its spectrum is being extracted. The same procedure is performed for every galaxy in the sample.

The result of extraction is the flux density spectrum ($S_{\nu_{obs}}$). This can be used to calculate the average HI mass ($\langle M_{HI} \rangle$), an important physical property. The flux density spectrum can be converted to an HI mass "spectrum" ($M_{HI,\nu_{obs}}$) via:

$$\left(\frac{M_{HI,\nu_{obs}}}{M_{\odot} MHz^{-1}}\right) = 4.98 \times 10^{7} \left(\frac{S_{\nu_{obs}}}{\text{Jy}}\right)\left(\frac{D_L}{\text{Mpc}}\right)^2, \tag{3.1}$$

where D_L is the luminosity distance of the galaxy. Due to the fact that every galaxy in the sample has a different optical redshift, their spectra have to be shifted to the rest frame (as illustrated in Figure 3.4). The aligning of spectra ensures that any channel containing HI signal is now at the rest frequency of the HI emission line ($\nu_0 = 1420.406$ MHz).

The frequency emitted by the galaxy in its rest frame, ν_{em}, is related to the observed frequency ν_{obs} via:

$$\nu_{em} = \nu_{obs}(1 + z), \tag{3.2}$$

where z is the redshift. The HI mass in rest frame must be conserved:

$$\int M_{HI,obs} d\nu_{obs} = \int M_{HI,em} d\nu_{em} \tag{3.3}$$

and is:

$$M_{HI,em} = \frac{M_{HI,obs}}{1 + z}, \tag{3.4}$$

where $M_{HI,em}$ is the mass of HI in the rest frame of the galaxy and $M_{HI,obs}$ is the mass in the observed frame.

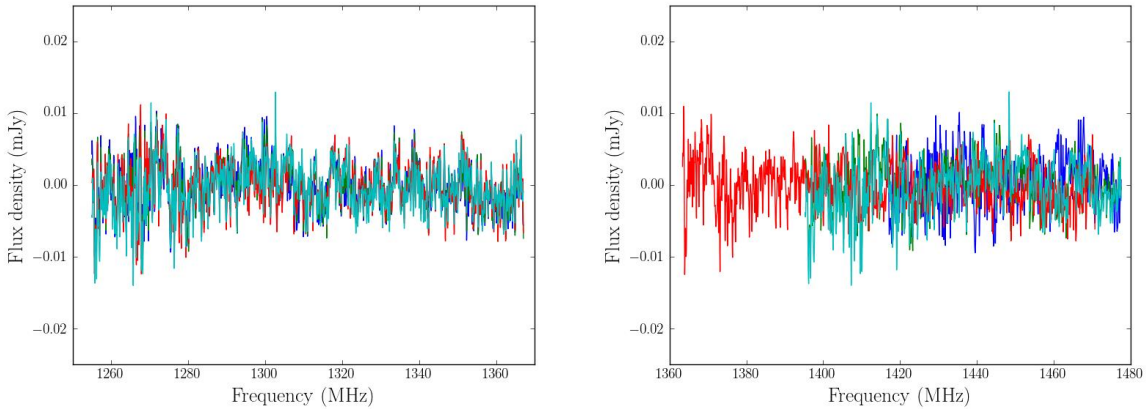

Figure 3.4: An example of 4 individual spectra extracted from the data cube. The figure shows these spectra before (left) and after (right) they are shifted to the rest frame. A strong, underlying ripple in spectrum, caused by proximity to continuum source, can be seen.

3.3 Stacking HI spectra

Once we obtain the shifted spectra, we "stack" by taking the weighted average via:

$$\langle X \rangle_\nu = \frac{\sum_{i=1}^{N} w_i X_{\nu,i}}{\sum_{i=1}^{N} w_i}, \tag{3.5}$$

where $\langle X \rangle_\nu$ is the stacked spectrum, $X_{\nu,i}$ is the spectrum of the i^{th} galaxy and w_i is the weight applied to the i^{th} spectrum. The X stands for S_ν (flux density spectrum), M_{HI} (HI mass spectrum) or M_{HI}/L_r (mass-to-light spectrum) used in our calculations. The mass-to-light spectrum is simply calculated by dividing the mass spectrum of the i^{th} galaxy by its luminosity.

The calculation of mass-to-light spectrum requires r-band luminosities (L_r) which are calculated from the absolute magnitudes (M_r) via:

$$L_r = 10^{0.4\left(M_{\odot,r} - M_r\right)}, \tag{3.6}$$

where $M_{\odot,r} = 4.71$ is the solar magnitude in r-band as in Hill et al. (2010) [48]. The absolute magnitudes provided by the GAMA stellar mass catalogue were derived using $\Omega_m = 0.3$, $\Omega_\Lambda = 0.7$, $h = 0.7$ cosmology. We convert them into the cosmology used in this thesis ($\Omega_m = 0.3$, $\Omega_\Lambda = 0.7$, $h = 1.0$) via:

$$M_{r,h=1.0} = M_{r,h=0.7} + 5\log\left(\frac{1.0}{0.7}\right). \tag{3.7}$$

The average luminosity $\langle L_r \rangle$ and corresponding error σ_{L_r} are calculated via:

$$\langle L_r \rangle = \frac{\sum_{i=1}^{N} L_{r,i}}{N}, \tag{3.8}$$

$$\sigma_{L_r} = \sqrt{\frac{\sum_{i=1}^{N} \sigma_{L_r,i}}{N}}, \tag{3.9}$$

where $L_{r,i}$ is the luminosity and $\sigma_{L_r,i}$ is the luminosity error of the i^{th} galaxy. The average luminosity of $N = 7049$ galaxies in the $G09$ field is $\langle L_r \rangle = (5.621 \pm 0.002) \times 10^9\ L_\odot$.

The applied weight (w_i) is calculated from the root mean squared (rms) noise level of the i^{th} spectrum (σ_i) using:

$$w_i = \sigma_i^{-2}, \tag{3.10}$$

This choice of weighting scheme maximizes the S/N we achieve in the final stacked spectrum.

Figure 3.5 shows how the number of co-added spectra (N) affects the S/N of the final stack. For small N, the high noise level prevents a statistical detection. As N increases, the noise level decreases and the statistical detection becomes more prominent. The success of the stacking experiment depends on the behavior of the rms noise. The best possible S/N is achieved when the noise behaves in a Gaussian manner, i.e. decreases with the square root of N. Figure 3.6 shows that the rms noise level of the stacked spectrum decreases with N. The noise behaves in a Gaussian manner, but slightly deviates probably due to residual RFI and continuum sources.

Deviation from the purely Gaussian behavior can occur due to the presence of radio frequency interference (RFI) and residual continuum emission in the data (see Figure 3.7). To account for RFI presence, we flag frequencies which contain known man-made narrow-band signals at 1312, 1316, 1349 and 1350 MHz. Continuum emission from astronomical sources may contaminate data by producing standing waves in the telescope structure which manifest as ripples in the spectral data [49]. Aligning of spectra at rest frame doesn't eliminate the ripple. The possible further influence of the continuum ripple on the final result will be discussed in the Section 3.6.

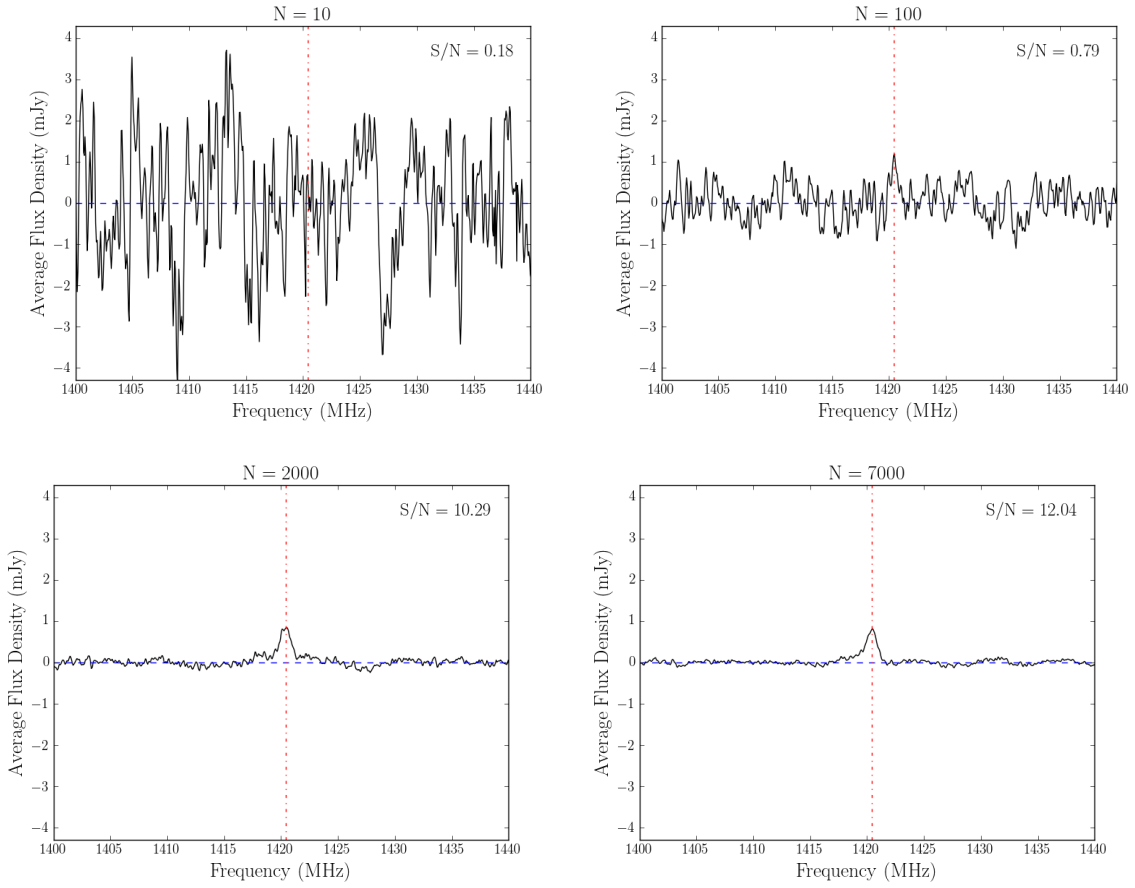

Figure 3.5: Stacking of N individual spectra. Noise dominates the stacked spectrum for small values of N and there is no statistical detection. As the number of stacked spectra grows, the noise decreases as the square root of N and the signal appears. Integrated S/N is quoted in upper right corners of figures.

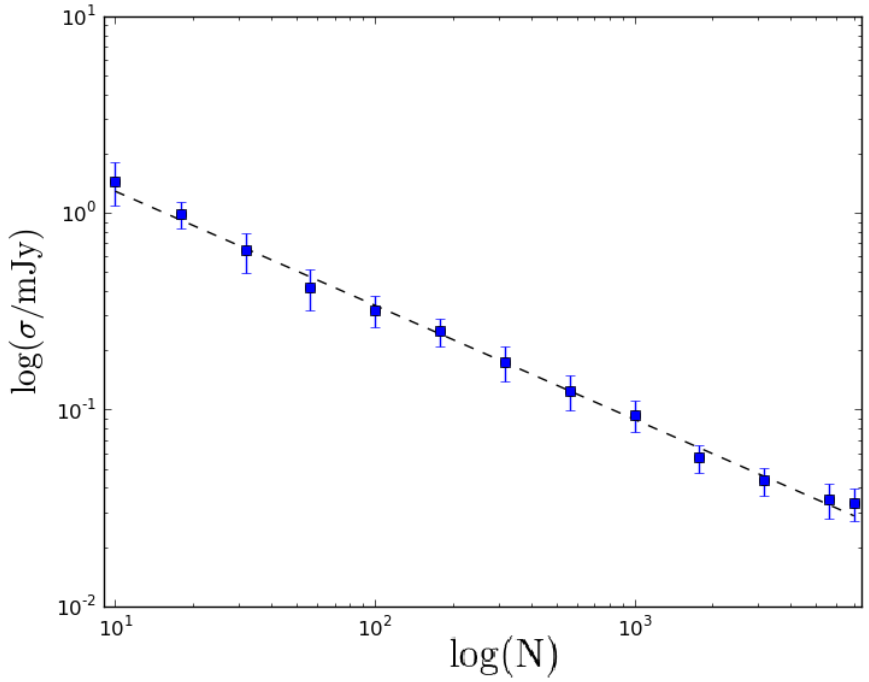

Figure 3.6: The rms noise level of the stacked spectrum versus the number of spectra being stacked. The linear fit gives gradient -0.58 ± 0.01, i.e. the noise decreases with the square root of number of stacked spectra.

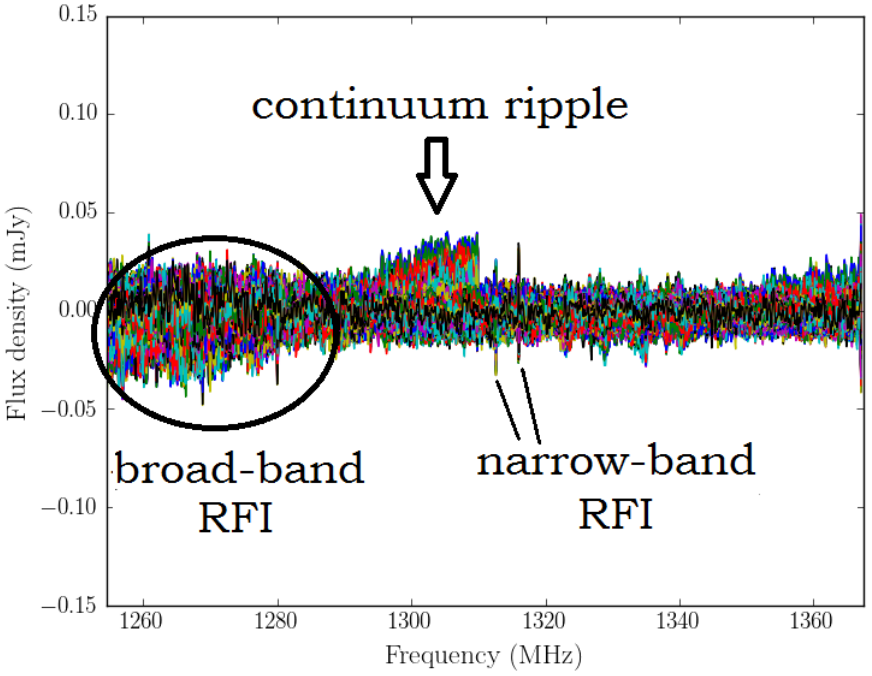

Figure 3.7: The RFI properties and spectral features of 7049 spectra extracted from the data cube.

The presence of this ripple can influence the shape of the baseline making it hard to identify appropriate bounds for integration of the stacked spectrum. This can result in poor estimate of average properties derived by integrating of the spectrum. In order to account for this problem, we fit a fourth–order polynomial baseline and then subtract it from the spectrum. This process is illustrated in Figure 3.8. The final results of stacking all 7049 sources is shown in Figure 3.9. It shows a strong statistical detection with $S/N = 11.89,\ 7.82,\ 4.05$ for the average flux spectrum, average mass spectrum and average mass-to-light spectrum, respectively.

As seen in Figure 3.9, the stacked spectra show asymmetry. This asymmetry could be present due to an insufficient baseline subtraction and the presence of continuum emission. It was also found by Delhaize et al. (2013) [37] that, whenever this asymmetry is present, it always tends to be towards lower frequencies. This occurrence is yet to be explained.

The stacking technique can be affected by the inaccurately determined spectroscopic redshifts [35]. Accurate redshifts are required for the proper alignment of non-detected galaxies. Large redshift errors may cause the *HI* stacked profile to be smeared out. The accuracy of GAMA-II redshifts is $27\ \mathrm{kms}^{-1}$, while the widths of the stacked spectra to be $600\ \mathrm{kms}^{-1}$. As found in simulations by Khandai et al. (2011), redshift errors $< 35\ \mathrm{kms}^{-1}$ dilute stacked profile by less than 3 percent [50]. Therefore, redshift errors are not expected to dominate the width of the stacked spectra obtained in this thesis.

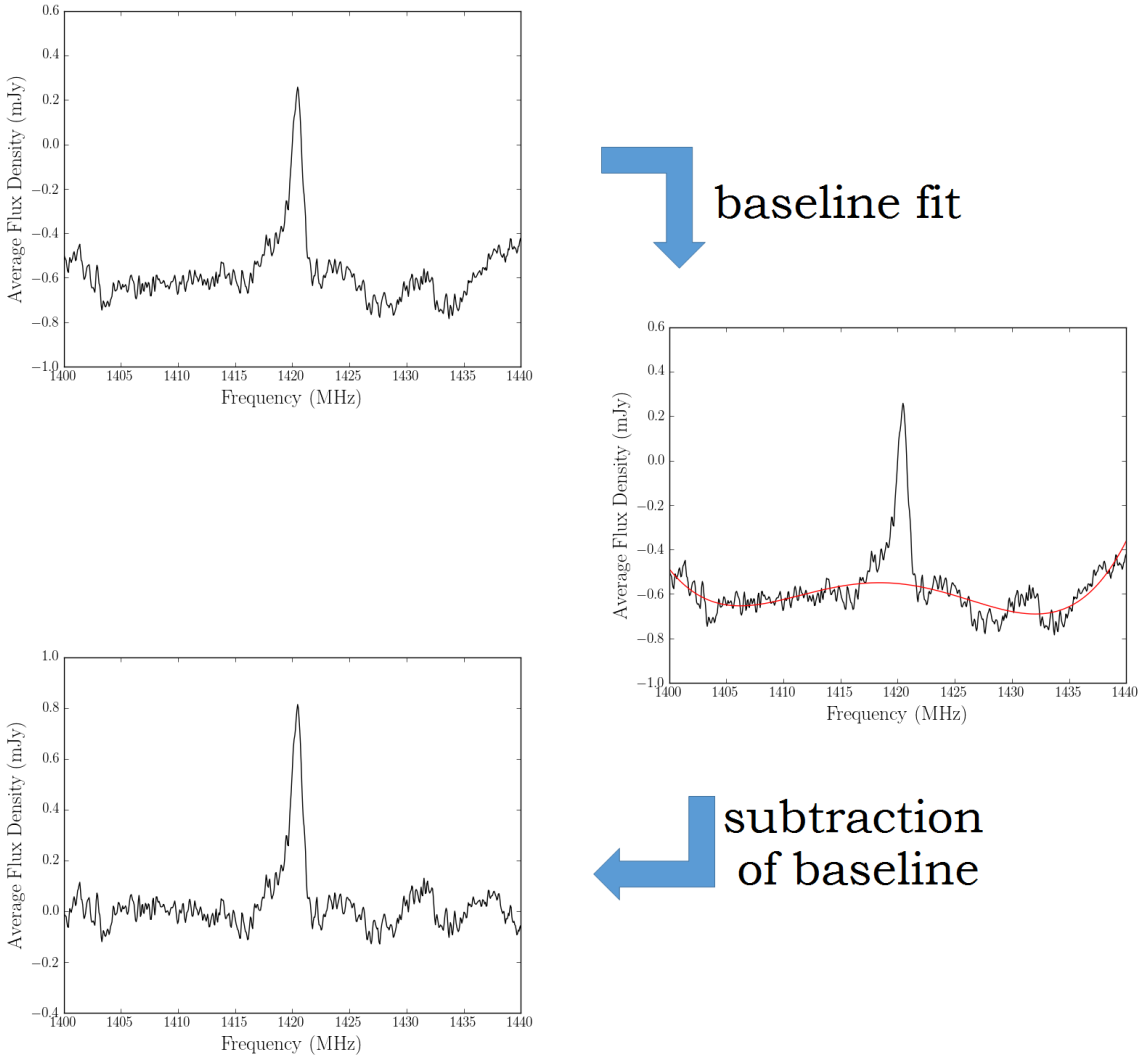

Figure 3.8: The process of baseline removal. A fourth-order polynomial baseline (red line) is fitted to the stacked spectra and then subtracted from it.

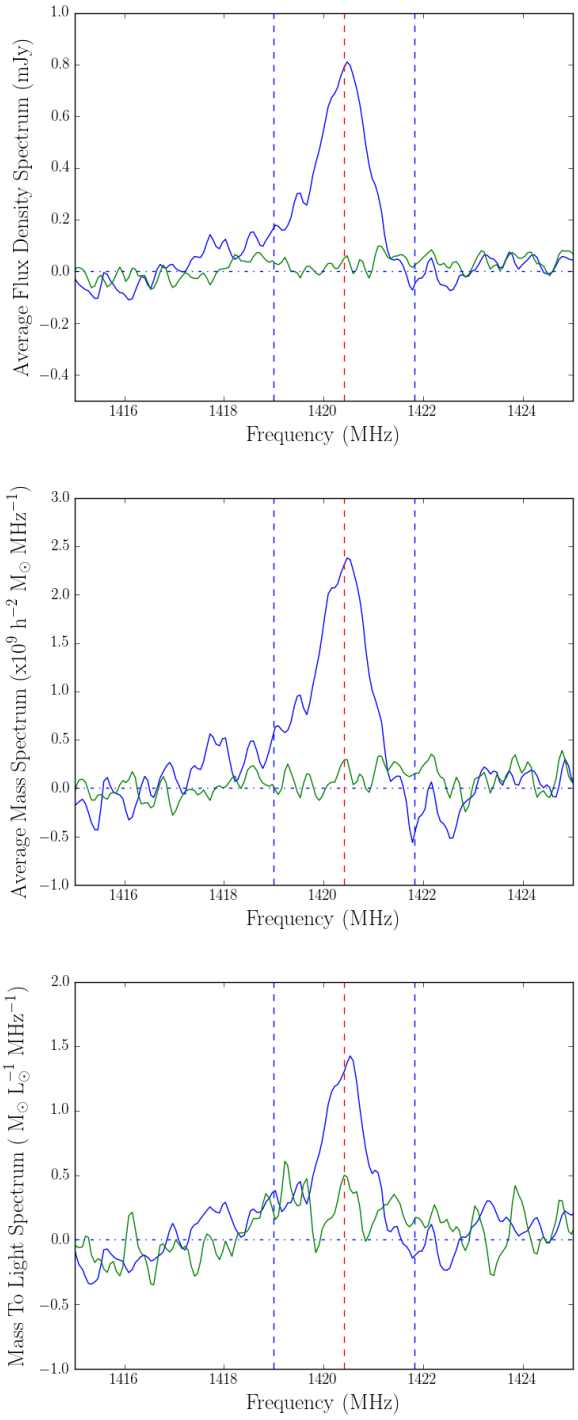

Figure 3.9: The average flux (top) and mass (middle) and mass–to–light (bottom) spectra (blue lines) obtained by the stacking technique. The green lines show an example of control spectrum to indicate the noise level, calculated by the procedure described in the text below. The vertical dashed blue lines show the integration limits and the vertical dashed red line shows the rest frame frequency, $\nu_0 = 1420.406$ MHz. Strong statistical detection can be seen in all tree spectra. Calculated integrated signal-to-noise ratios are: 11.89 for average flux spectrum, 7.82 for average mass spectrum and 4.05 for mass-to-light spectrum.

3.4 Average HI properties derived from stacking

The average properties of HI gas are found by integrating the stacked spectrum over the frequency range of the co-added profile using the formula:

$$\langle X \rangle = \int_{\nu_{em,1}}^{\nu_{em,2}} \langle X \rangle_{\nu_{em}} d\nu_{em}, \tag{3.11}$$

where the limits are $\nu_{em1,2} = \nu_0 \mp 1.42$ MHz and are indicated in Figure 3.9. As before X stands for S_ν (flux density spectrum), M_{HI} (HI mass spectrum) or M_{HI}/L_r (mass-to-light spectrum). These bounds were chosen based on the results of Obreschkow et al (2013) [51] whose simulations show that the expected maximum width for any individual galaxy is $600\ \mathrm{kms}^{-1}$.

$\langle \boldsymbol{S} \rangle [\mathbf{mJy}]$	$\langle \boldsymbol{M_{HI}} \rangle [\times \mathbf{10^9 M_\odot h^{-2}}]$	$\left\langle \frac{\boldsymbol{M_{HI}}}{\boldsymbol{L_r}} \right\rangle \left[\frac{\boldsymbol{M_\odot}}{\boldsymbol{L_\odot}} \right]$
(1.07 ± 0.09)	(2.97 ± 0.38)	(1.58 ± 0.39)

Table 3.1: Average properties of the HI gas derived using the stacking technique. Average flux density (left), average mass (center) and average mass-to-light ratio (right).

Average HI properties obtained by the stacking analysis are shown in the Table 3.1. These values are overestimated due to confusion effect, described in Section 3.5. The average HI mass for 7049 galaxies is $\langle M_{HI} \rangle = (2.97 \pm 0.38) \times 10^9 M_\odot h^{-2}$. This sample appears to have average masses below the characteristic mass $M^* = (3.55 \pm 0.04) \times 10^9 M_\odot h^{-2}$ presented in Zwaan et al. (2005) [17], and well below the average mass $\langle M_{HI} \rangle = (6.93 \pm 0.17) \times 10^9 M_\odot h^{-2}$ over the same redshift range presented in Delhaize et al. (2013) [37].

The errors on the average HI properties presented in Table 3.1, are estimated by creating ten control catalogues. Each catalogue is generated by randomly mismatching redshifts of the GAMA objects with their positions. Since we use "incorrect" redshifts for each source, stacking of these spectra produces no statistical detection. However, this method provides information on the noise behavior and enables us to calculate errors on integrated values as the standard deviation of integrated values (obtained by using Eq. 3.11) of all ten catalogues.

3.5 Confusion

As mentioned before, confusion occurs when there are many individual galaxies at similar redshifts located within the beam of the telescope. This may lead us to integrate over multiple HI profiles per spectrum, therefore overestimating the average HI mass and the average HI mass-to-light ratio. Since we cannot deconvolve the HI spectrum that comes from certain galaxies within the beam of the Parkes telescope (15.5 arcmin), we approximate the confusion factor $\mathcal{C}$ with which we artificially boost luminosities to counteract the effect of confusion.

We have calculated the number of galaxies that are located within the radius 15.5 arcmin from the i^{th} galaxy with redshifts $z_i \pm 0.002$, where z_i is the redshift of the i^{th} galaxy. By taking the average of the number of galaxies that obey these conditions, we get a mean value of 8.6, i.e. every one galaxy is confused by ~9 others. The distribution of the number of confused galaxies within the beam of the Parkes telescope is shown in Figure 3.10. We define the confusion factor $\mathcal{C}$ as:

$$\mathcal{C} = 8.6. \tag{3.12}$$

This procedure is less sophisticated than the one used in Delhaize et al. (2013) [37] but serves as a good estimate of the effect confusion has on our results. Figure 3.11 the distribution of original and artificially-boosted luminosities as a means of counteracting the overestimated average HI properties.

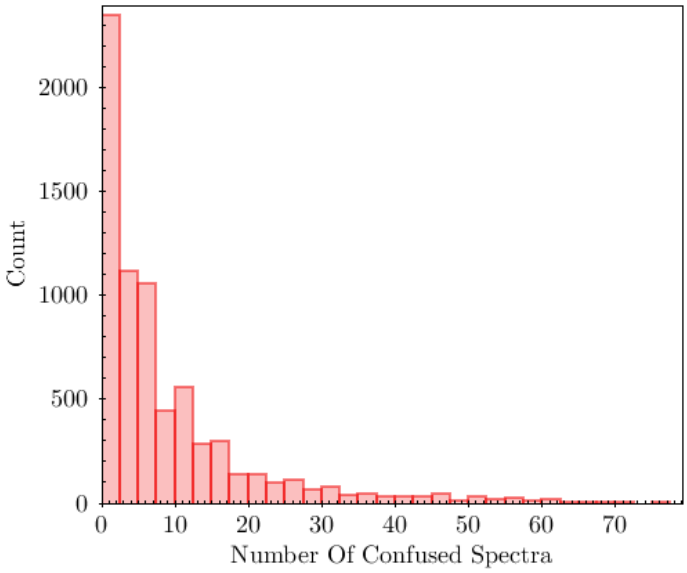

Figure 3.10: Distribution of the number of confused galaxies within the beam width of the Parkes telescope for the sample of 7049 galaxies. The average number of confused spectra is 8.6. The maximum number of confused spectra is 75.

Mass-to-light ratio corrected for confusion from this thesis is $\langle M_{HI}/L_r \rangle = (0.18 \pm 0.05)\ M_\odot/L_\odot$, smaller by the factor of 2 from $\langle M_{HI}/L_r \rangle = (0.32 \pm 0.02)\ M_\odot/L_\odot$ as presented in Delhaize et al. (2013) [37]. This was expected because we are sampling GAMA objects which are fainter, i.e. have smaller total *HI* masses, than the 2dFGRS objects from Delhaize et al. (2013). Also, by using this confusion correction scheme, we are overestimating luminosities, hence underestimating average *HI* mass-to-light ratio.

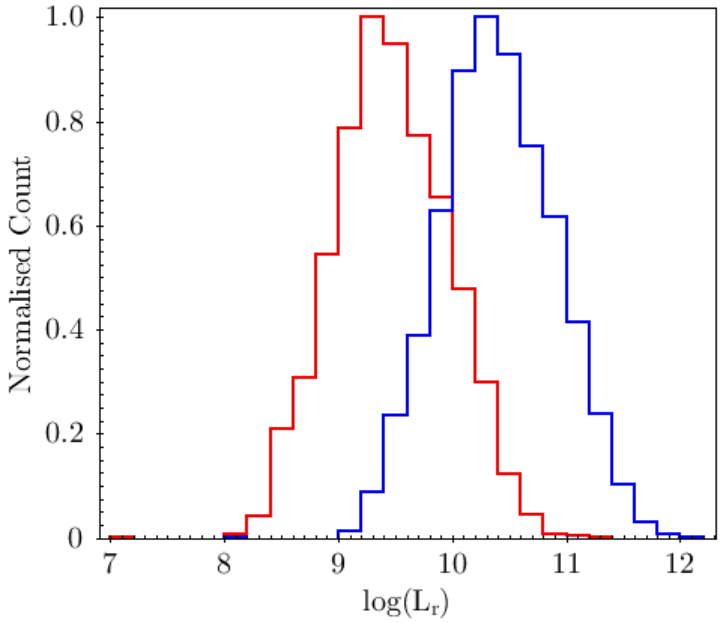

Figure 3.11: The luminosity distribution of stacked sources before (red) and after (blue) confusion correction. We boost luminosities in order to counteract the effect confusion have on average *HI* properties.

3.6 Calculation of cosmic HI mass density

We use two schemes with different form of average mass-to-light ratios to calculate Ω_{HI}. We are testing these methods to see how they compare when applied to the same data sets.

The first method, adopted from Delhaize et al. (2013) [37], uses average *HI* mass-to-light ratio via:

$$\Omega_{HI1} = \left\langle \frac{M_{HI}}{L_r} \right\rangle \frac{1}{\mathcal{C}} \times \frac{\rho_{L_r}}{\rho_c}. \tag{3.13}$$

The second was adopted from Rhee et al. (2013) [38] and it uses the ratio of average HI mass and average luminosities:

$$\Omega_{HI2} = \frac{\langle M_{HI} \rangle}{\langle L_r \rangle \mathcal{C}} \times \frac{\rho_{L_r}}{\rho_c}, \tag{3.14}$$

In both schemes $\rho_c = 3H_0^2/8\pi G \approx 2.78 \times 10^{11}\, M_\odot\, h^2\, Mpc^{-3}$ is the critical density of the Universe, $\rho_{L_r} = (2.29 \pm 0.06) \times 10^8 L_\odot\, h\, Mpc^{-3}$ is the luminosity density in r band [52] and $\mathcal{C}$ is the confusion factor.

Calculated values of the cosmic HI mass densities are shown in Table 3.2 and listed in Table 3.3 for comparison with literature values.

	No correction $\mathcal{C} = 1$	**Corrected for confusion** $\mathcal{C} = 8.6$
$\boldsymbol{\Omega_{HI1} \times 10^{-4} h^{-1}}$	13.02 ± 3.24	1.51 ± 0.38
$\boldsymbol{\Omega_{HI2} \times 10^{-4} h^{-1}}$	4.35 ± 0.56	0.51 ± 0.07

Table 3.2: Calculated cosmic HI mass densities obtained by using methods 1 and 2 for cases without (1^{st} column) and with (2^{nd} column) confusion correction.

3.7 Discussion

By using the technique of spectral stacking we made high-significance stacked detections, showing that stacking is an efficient method of obtaining statistical detections of individually-undetected sources. Since we are not restricted to regions where direct detections are obtainable, stacking allows us to study larger volumes of sky than otherwise possible, thus minimizing the effect cosmic variance has on our measurements.

We conclude that the two methods we use of calculating Ω_{HI} (see Section 3.6) do not provide consistent results. Delhaize et al. (2013) [37] and Rhee et al. (2013) [38] suggest different correction factors to account for the fact that the luminosity distribution of the galaxy sample being stacked may not represent the true luminosity distribution of all galaxies at the studied redshift. Delhaize (2014) [46] found that weighting factors, applied to mean mass-to-light ratios, can differ greatly between these two methods. We have not applied such a correction to our values. This is most likely explanation for the discrepancy between the two methods in our results.

The Ω_{HI} estimates which are not corrected for confusion are much higher than other literature values, especially the result calculated via eq. 3.13. As described in Section 3.5, this is expected due to confusion, which leads us to overestimate HI masses. The corrected values are lower than other literature values at the same redshift. This may be due to an overestimation of the correction for confusion. By assuming that any galaxy within $\pm 300\ \mathrm{kms}^{-1}$ and within one beam width of the telescope is confused, the extent confusion has on our data is perhaps overestimated as the variety of HI profile widths in galaxies may be much smaller than the maximum expected value of $600\ \mathrm{kms}^{-1}$ [51]. Clearly confusion plays a big role and makes interpretation of the results difficult. More advanced method of correcting for confusion will be discussed in Section 4.2.

It is most likely that the "true" Ω_{HI} value lies somewhere between the corrected and uncorrected values from this thesis, in accordance to the literature results (from Delhaize et al. (2013) [37], Rhee et al. (2013) [38], Freudling et al. (2011) [20], Hoppmann et al. (2015) [21]). This would imply little or no evolution of Ω_{HI} out to $z = 0.134$ (the past $\sim$1.67 Gyr). As seen from literature values and simulations in Figure 3.12, there is very little evolution of Ω_{HI} out to

$z\sim10$, compared to the evolution of SFR. This may be explained by the feedback processes which replace the gas which previously fueled star formation.

Source	$< z >$	z_{min}	z_{max}	$\Omega_{HI}\left(\times 10^{-4}h^{-1}\right)$	***Method***
Zwaan et al. (2005)	0.015	0.001	0.0423	2.6 ± 0.3	Direct Detection
Martin et al. (2010)	0.026	0	0.052	3.0 ± 0.2	Direct Detection
Delhaize et al. (2013)	0.028	0	0.04	$2.82^{+0.3}_{-0.59}$	Stacking
Hoppmann et al. (2015)	0.065	0	0.132	2.33 ± 0.07	Direct Detection
This thesis$_1$	**0.086**	**0.039**	**0.134**	$\mathbf{13.02 \pm 3.24}$	**Stacking**
This thesis$_1^{\mathcal{C}}$				$\mathbf{1.51 \pm 0.38}$	
This thesis$_2$				$\mathbf{4.35 \pm 0.53}$	
This thesis$_2^{\mathcal{C}}$				$\mathbf{0.51 \pm 0.07}$	
Delhaize et al. (2013)	0.096	0.04	0.13	$3.19^{+0.43}_{-0.59}$	Stacking
Rhee et al. (2013)	0.1	0.1	0.1	2.31 ± 0.35	Stacking
Freudling et al. (2011)	0.125	0.125	0.125	3.4 ± 1.1	Direct Detection
Rhee (2013)	0.2	0.2	0.2	2.38 ± 0.63	Stacking
Lah et al. (2007)	0.24	0.24	0.24	4.9 ± 2.2	Stacking
Rao et al. (2006)	0.505	0.11	0.9	5.2 ± 1.9	DLAs
Masui et al. (2013)	0.8	0.8	0.8	3.03 ± 0.56	Intensity Mapping
Rao et al. (2006)	1.275	0.9	1.65	5.1 ± 1.5	DLAs
Prochaska & Wolfe (2009)	2.31	2.2	2.4	2.78 ± 0.48	DLAs
Prochaska & Wolfe (2009)	2.57	2.4	2.7	$3.73^{+0.41}_{-0.43}$	DLAs
Prochaska & Wolfe (2009)	2.86	2.7	3.0	3.73 ± 0.39	DLAs
Prochaska & Wolfe (2009)	3.7	3.5	4.0	$6.07^{+1.05}_{-1.06}$	DLAs
Crighton et al. (2015)	4.005	3.56	4.45	8.26 ± 1.82	DLAs
Prochaska & Wolfe (2009)	4.39	4.0	5.5	$5.9^{+1.26}_{-1.11}$	DLAs
Crighton et al. (2015)	4.88	4.45	5.31	$6.86^{+1.4}_{-1.26}$	DLAs

Table 3.3: Values of Ω_{HI} from the literature. All values have been converted to the cosmology $h = 1.0$ $\Omega_\Lambda = 0.7$ and $\Omega_M = 0.3$. Ω_{HI} values obtained in this thesis have indices 1 and 2, corresponding to eq. 3.13 and eq. 3.14 from which they are calculated. Index $\mathcal{C}$ indicated results which were corrected for confusion. All values from this table are shown in Figure 3.12.

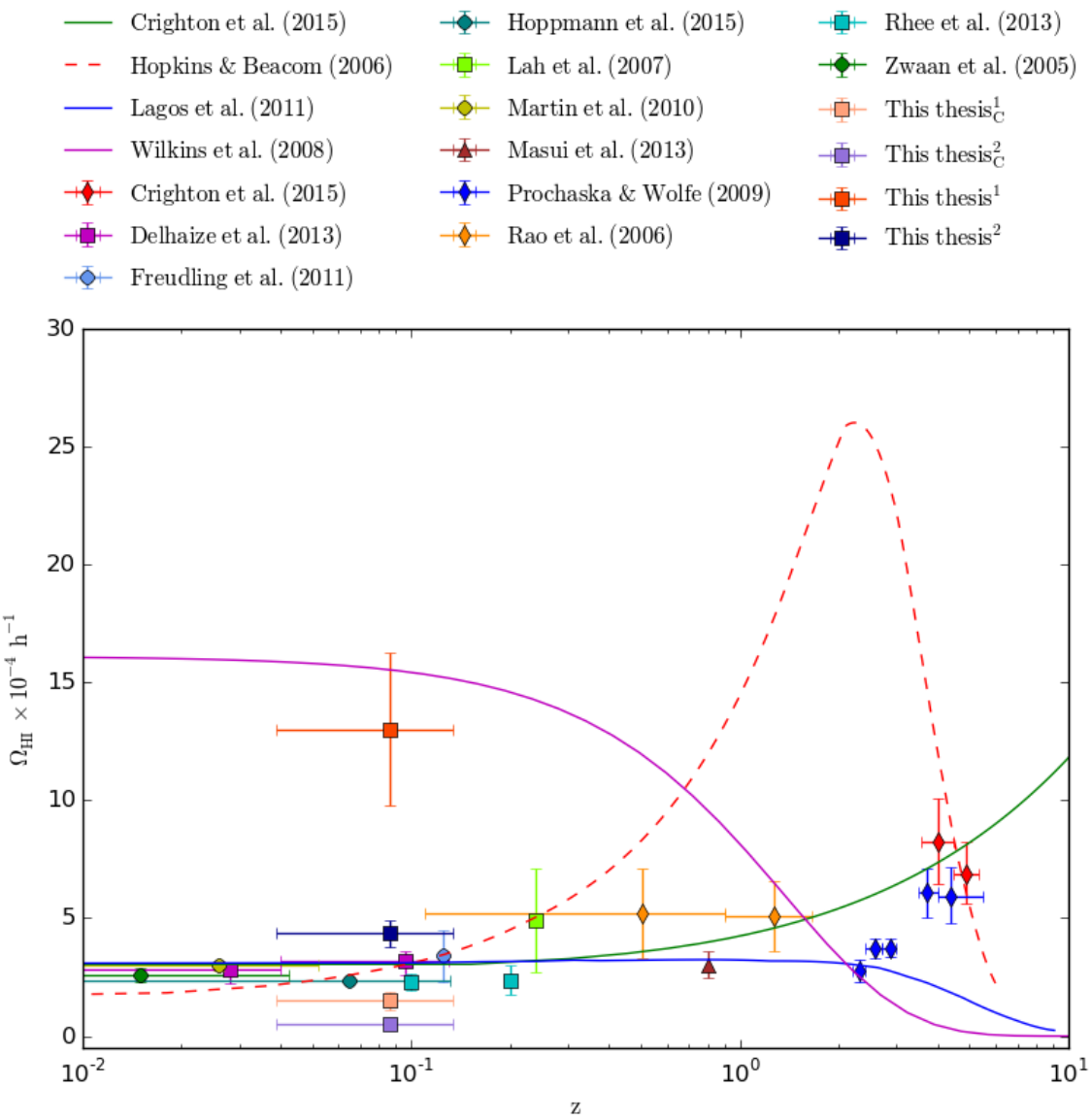

Figure 3.12: The cosmic HI mass density Ω_{HI} versus redshift. Observational measurements from the literature are indicated in the legend and shown in a plot as points. Measurements obtained by simulations show the evolution of the cosmic stellar mass density (solid pink line) [14], the evolution of the cosmic star formation rate density scaled by the factor of $10^{9.5}$ (the dashed red line) [13], the semi-analytical prediction of the Ω_{HI} evolution (solid blue line) [15] and the power-law fitting to the literature data (solid green line) [16]. The results of this thesis are shown with red and orange squares (results of method 1 and 2, respectively, without confusion correction) and pink and purple squares (results of confusion corrected method 1 and 2, respectively).

4 Summary and outlook

4.1 Summary

This thesis presents a spectral stacking analysis of the neutral hydrogen (HI) gas properties in distant galaxies. Cold ($< 10^4$K) HI gas is a precursor of molecular hydrogen, the fuel for the star formation, and thus plays an important role in galaxy evolution. The HI content of galaxies in the nearby Universe can be traced via direct detection of the 21 cm hyperfine emission line. At high redshifts, HI can be indirectly detected using damped Lyman α systems. Direct detections are restricted to low redshifts due to technical limitations of currently available generation of telescopes. On the other hand, DLA measurements become difficult at $z < 1.65$ because their spectra shifts to UV and cannot be detected from the Earth's surface. To bridge the gap in measurements at intermediate redshifts, we use the statistical technique of spectral stacking which enables us to examine average HI properties over the large volumes of sky.

For the stacking analysis presented here, we use positions and spectroscopic redshifts provided by the GAMA survey to identify where galaxies are within an HI data cube recorded with the Parkes 64m telescope. Once we identify galaxies, we extract their spectra and shift them to rest frame. We co-add the HI spectra of 7049 galaxies within the 60 deg^2 $G09$ field centered at RA 9^h within the redshift range $0.039 < z < 0.134$. We obtained stacked spectra with strong statistical detections and high integrated signal-to-noise ratios of $S/N = 11.9$. The rms noise in the stacked signal appears to display Gaussian behavior, i.e. decrease with the square root of the number of stacked spectra. Stacked spectra show asymmetry towards lower frequencies, the occurrence of which is yet to be explained but could be due to non-Gaussian noise components remaining in the data.

From the stacked spectra, we measure the average flux density, average HI mass and average HI mass-to-light ratio. Respectively, these are: $\langle S \rangle = (1.07 \pm 0.09)$ mJy, $\langle M_{HI} \rangle = (2.97 \pm 0.38) \times 10^9 M_\odot h^{-2}$ and $\langle M_{HI}/L_r \rangle = (1.58 \pm 0.39)\, M_\odot L_\odot^{-1}$. A correction for source confusion has been applied to these values. Confusion is an effect that appears due to the fact that we cannot deconvolve the HI contributions from multiple galaxies within the Parkes beam (15.5 arcmin), hence end up integrating over several HI spectra and overestimating calculated average HI properties. We calculate the average number of galaxies within a radius of 15.5 arcmin and with redshift ± 0.002 ($\Delta v = \pm 300$ kms^{-1}) of each galaxy to be 8.6. We define

the confusion factor as $\mathcal{C} = 8.6$. To obtain average mass-to-light values corrected for confusion, we multiply luminosities by the average confusion factor 8.6, thus artificially boosting them to counteract the effect of a confused average HI mass and average HI mass-to-light ratio.

We use two strategies to derive the cosmic HI mass density (Ω_{HI}) over our observed redshift range in order to test their consistency. The first uses the average HI mass-to-light ratio ($\langle M_{HI}/L_r \rangle$) and produces the result $\Omega_{HI} = (1.51 \pm 0.38) \times 10^{-4} h^{-1}$. The second strategy uses the ratio of the average HI mass and the average of the r-band luminosities ($\langle M_{HI} \rangle / \langle L_r \rangle$) and resulted in $\Omega_{HI} = (0.51 \pm 0.07) \times 10^{-4} h^{-1}$. We find that these methods don't give consistent results, due to inadequate confusion correction and an additional factor required to correct for the underlying luminosity distribution. The applied confusion correction is likely too extreme, and hence our Ω_{HI} estimates are significantly lower than other values from the literature.

As seen from measurements by Delhaize et al. (2013) [37], Rhee et al. (2013) [38], Freudling et al. (2011) [20], Hoppmann et al. (2015) [21], and from the Lagos et al. (2011) [15] simulation of Ω_{HI} evolution, it is not likely that there has been evolution of Ω_{HI} over the redshift range $0.039 < z < 0.134$, despite the evolution of the star formation rate. Mild evolution of Ω_{HI} is consistent with the ΛCDM picture according to which the HI content of galaxies is replenished through various accretion and feedback processes.

4.2 Future work

The results of this thesis could be improved by excluding continuum sources and using a more sophisticated method of confusion correction. Continuum sources in the $G09$ field could be identified by using one of the continuum surveys, such as Faint Images of the Radio Sky at Twenty-cm (FIRST) [53] and NRAO VLA Sky Survey (NVSS) [54]. Once we identify those sources, we could exclude all data within a beam width of any continuum source with higher flux density greater than 200 mJy at 1.4 GHz. This might remove the continuum ripple from spectra extracted from the data cube and reduce asymmetry observed in stacked spectra.

The issue of source confusion results from the large (15.5 arcmin) beam size of the single-dish Parkes telescope. One approach would be to use a more sophisticated calculation of the confusion effect, as in Delhaize et al. (2013) [37]. They estimated the average HI profile widths of the galaxies using the Tully-Fisher relation in their samples and used those values to

artificially confuse luminosities on a galaxy-by-galaxy basis. By doing so, the extent of confusion would not be overestimated to the degree seen in this thesis, hence obtained Ω_{HI} values would be closer to their actual values. The other approach to overcome the confusion problem would be to use a radio interferometer, such as the Karl G. Jansky Very Large Array (VLA) or the Australia Telescope Compact Array (ATCA). Follow-up observations with these instruments would provide data with little or no source confusion due to their high angular resolutions ($\sim$1 arcsec).

References

[1] H. Mo, F. C. van den Bosch, S. White. Galaxy Formation and Evolution, Cambridge University Press, 2010.

[2] Planck Collaboration, R. Adam et al. Planck 2015 results. I. Overview of products and scientific results. // *ArXiv e-prints*, February 2015.

[3] A. H. Guth. Inflationary universe: A possible solution to the horizon and flatness problems. // 23:347–356, January 1981.

[4] S. Cole, C. G. Lacey, C. M. Baugh, and C. S. Frenk. Hierarchical galaxy formation. // 319:168–204, November 2000.

[5] T. Di Matteo, V. Springel, and L. Hernquist. Energy input from quasars regulates the growth and activity of black holes and their host galaxies. // 433:604–607, February 2005.

[6] G. Efstathiou. A model of supernova feedback in galaxy formation. // 317:697–719, September 2000.

[7] D. J. Griffiths. Hyperfine splitting in the ground state of hydrogen. // *American Journal of Physics*, 50:698–703, August 1982

[8] HIPASS Public Data Release, Australia Telescope National Facility, http://www.atnf.csiro.au/research/multibeam/release/, 25.08.2015.

[9] B. S. Koribalski et al. The 1000 Brightest HIPASS Galaxies: H I Properties. // 128:16–46, July 2004.

[10] L. Staveley-Smith. HI Multibeam Survey Techniques. // 14:111–116, April 1997.

[11] M. P. Haynes, L. van Zee, D. E. Hogg, M. S. Roberts, and R. J. Maddalena. Asymmetry in high-precision global H I profiles of isolated spiral galaxies. // 115:62, January 1998.

[12] R. Sancisi. Warped HI Disks in Galaxies. // 53:159, December 1976.

[13] A. M. Hopkins and J. F. Beacom. On the Normalization of the Cosmic Star Formation History. // 651:142–154, November 2006.

[14] S. M. Wilkins, N. Trentham, and A. M. Hopkins. The evolution of stellar mass and the implied star formation history. // 385:687–694, April 2008.

[15] C. D. P. Lagos, C. M. Baugh, C. G. Lacey, A. J. Benson, H.-S. Kim, and C. Power. Cosmic evolution of the atomic and molecular gas contents of galaxies. // 418:1649–1667, December 2011.

[16] N. H. M. Crighton, M. T. Murphy, J. X. Prochaska, G. Worseck, M. Rafelski, G. D. Becker, S. L. Ellison, M. Fumagalli, S. Lopez, A. Meiksin, and J. M. O'Meara. The neutral hydrogen cosmological mass density at $z = 5$. // 452:217–234, September 2015.

[17] M. A. Zwaan, M. J. Meyer, L. Staveley-Smith, and R. L. Webster. The HIPASS catalogue: Ω_{HI} and environmental effects on the HI mass function of galaxies. // 359:L30–L34, May 2005.

[18] M. J. Meyer et al. The HIPASS catalogue - I. Data presentation. // 350:1195–1209, June 2004.

[19] A. M. Martin, E. Papastergis, R. Giovanelli, M. P. Haynes, C. M. Springob, and S. Stierwalt. The Arecibo Legacy Fast ALFA Survey. X. The H I Mass Function and Ω_{HI} from the 40% ALFALFA Survey. // 723:1359–1374, November 2010.

[20] W. Freudling, L. Staveley-Smith, B. Catinella, R. Minchin, M. Calabretta, E. Momjian, M. Zwaan, M. Meyer, and K. O'Neil. Deep 21 cm H I Observations at $z\sim0.1$: The Precursor to the Arecibo Ultra Deep Survey. // 727:40, January 2011.

[21] L. Hoppmann, L. Staveley-Smith, W. Freudling, M. A. Zwaan, R. F. Minchin, and M. R. Calabretta. A blind H I mass function from the Arecibo Ultra-Deep Survey (AUDS). // 452:3726–3741, October 2015.

[22] X. Fernández, et al. A Pilot for a Very Large Array H I Deep Field. // 770:L29, June 2013.

[23] L. J. Storrie-Lombardi and A. M. Wolfe. Surveys for z3 Damped Lyα Absorption Systems: The Evolution of Neutral Gas. // 543:552–576, November 2000.

[24] J. X. Prochaska, S. Herbert-Fort, and A. M. Wolfe. The SDSS Damped Lyα Survey: Data Release 3. // 635:123–142, December 2005.

[25] J. X. Prochaska and A. M. Wolfe. On the (Non)Evolution of H I Gas in Galaxies Over Cosmic Time. // 696:1543–1547, May 2009.

[26] M. A. Zwaan, P. G. van Dokkum, and M. A. W. Verheijen. Hydrogen 21-Centimeter Emission from a Galaxy at Cosmological Distance. // *Science*, 293:1800–1803, September 2001.

[27] M. Verheijen, J. H. van Gorkom, A. Szomoru, K. S. Dwarakanath, B. M. Poggianti, and D. Schiminovich. WSRT Ultradeep Neutral Hydrogen Imaging of Galaxy Clusters at $z\sim0.2$: A Pilot Survey of Abell 963 and Abell 2192. // 668:L9–L13, October 2007.

[28] B. Catinella, M. P. Haynes, R. Giovanelli, J. P. Gardner, and A. J. Connolly. A Pilot Survey of H I in Field Galaxies at Redshift $z\sim0.2$. // 685:L13–L17, September 2008.

[29] U.-L. Pen, L. Staveley-Smith, J. B. Peterson, and T.-C. Chang. First detection of cosmic structure in the 21-cm intensity field. // 394:L6–L10, March 2009.

[30] T.-C. Chang, U.-L. Pen, K. Bandura, and J. B. Peterson. Hydrogen 21-cm Intensity Mapping at redshift 0.8. // *ArXiv e-prints*, July 2010.

[31] K. W. Masui, E. R. Switzer, N. Banavar, K. Bandura, C. Blake, L.-M. Calin, T.-C. Chang, X. Chen, Y.-C. Li, Y.-W. Liao, A. Natarajan, U.-L. Pen, J. B. Peterson, J. R. Shaw, and T. C. Voytek. Measurement of 21 cm Brightness Fluctuations at $z\sim0.8$ in Cross-correlation. // 763:L20, January 2013.

[32] J. N. Chengalur, R. Braun, and M. Wieringa. HI in Abell 3128. // 372:768–774, June 2001.

[33] P. Lah, M. B. Pracy, J. N. Chengalur, F. H. Briggs, M. Colless, R. de Propris, S. Ferris, B. P. Schmidt, and B. E. Tucker. The HI gas content of galaxies around Abell 370, a galaxy cluster at $z = 0.37$. // 399:1447–1470, November 2009.

[34] S. Fabello, G. Kauffmann, B. Catinella, R. Giovanelli, M. P. Haynes, T. M. Heckman, and D. Schiminovich. Arecibo Legacy Fast ALFA H I data stacking - II. H I content of the host galaxies of active galactic nuclei. // 416:1739–1744, September 2011.

[35] N. Maddox, K. M. Hess, S.-L. Blyth, and M. J. Jarvis. Comparison of H I and optical redshifts of galaxies - the impact of redshift uncertainties on spectral line stacking. , 433:2613–2625, August 2013.

[36] P. Lah, J. N. Chengalur, F. H. Briggs, M. Colless, R. de Propris, M. B. Pracy, W. J. G. de Blok, S. S. Fujita, M. Ajiki, Y. Shioya, T. Nagao, T. Murayama, Y. Taniguchi, M. Yagi, and S. Okamura. The HI content of star-forming galaxies at $z = 0.24$. // 376:1357–1366, April 2007.

[37] J. Delhaize, M. J. Meyer, L. Staveley-Smith, and B. J. Boyle. Detection of H I in distant galaxies using spectral stacking. // 433:1398–1410, August 2013.

[38] J. Rhee, M. A. Zwaan, F. H. Briggs, J. N. Chengalur, P. Lah, T. Oosterloo, and T. van der Hulst. Neutral atomic hydrogen (H I) gas evolution in field galaxies at $z\sim0.1$ and 0.2. // 435:2693–2706, November 2013.

[39] J. Liske et al. Galaxy And Mass Assembly (GAMA): end of survey report and data release 2. // 452:2087–2126, September 2015.

[40] S. P. Driver et al. GAMA: towards a physical understanding of galaxy formation. // *Astronomy and Geophysics*, 50(5):12–5, October 2009.

[41] S. P. Driver et al. Galaxy and Mass Assembly (GAMA): survey diagnostics and core data release. // 413:971–995, May 2011.

[42] I. K. Baldry et al. Galaxy And Mass Assembly (GAMA): AUTOZ spectral redshift measurements, confidence and errors. // 441:2440–2451, July 2014.

[43] E. N. Taylor et al. Galaxy And Mass Assembly (GAMA): stellar mass estimates. // 418:1587–1620, December 2011.

[44] J. Delhaize et al. GAMA: Studying HI properties of galaxies to $z = 0.1$ with spectral stacking. // In preparation.

[45] L. Staveley-Smith, W. E. Wilson, T. S. Bird, M. J. Disney, R. D. Ekers, K. C. Freeman, R. F. Haynes, M. W. Sinclair, R. A. Vaile, R. L. Webster, and A. E. Wright. The Parkes 21 CM multibeam receiver. // 13:243–248, November 1996.

[46] J. Delhaize. Studies of Galaxy Evolution Using Stacking Technique. PhD thesis. University of Western Australia, 2014

[47] R. J. Sault, P. J. Teuben, and M. C. H. Wright. A Retrospective View of MIRIAD. In R. A. Shaw, H. E. Payne, and J. J. E. Hayes, editors, *Astronomical Data Analysis Software and Systems IV*. // Volume 77 of *Astronomical Society of the Pacific Conference Series*, page 433, 1995.

[48] D. T. Hill, S. P. Driver, E. Cameron, N. Cross, J. Liske, and A. Robotham. The ugrizYJHK luminosity distributions and densities from the combined MGC, SDSS and UKIDSS LAS data sets. // 404:1215–1230, May 2010.

[49] D. G. Barnes et al. The HI Parkes All Sky Survey: southern observations, calibration and robust imaging. // 322:486–498, April 2001.

[50] N. Khandai, S. K. Sethi, T. Di Matteo, R. A. C. Croft, V. Springel, A. Jana, and J. P. Gardner. Detecting neutral hydrogen in emission at redshift $z\sim1$. // 415:2580–2593, August 2011.

[51] D. Obreschkow, X. Ma, M. Meyer, C. Power, M. Zwaan, L. Staveley-Smith, and M. J. Drinkwater. Confronting Cold Dark Matter Predictions with Observed Galaxy Rotations. // 766:137, April 2013.

[52] S. P. Driver et al. Galaxy And Mass Assembly (GAMA): the $0.013 < z < 0.1$ cosmic spectral energy distribution from 0.1 μm to 1 mm. // 427:3244–3264, December 2012.

[53] R. H. Becker, R. L. White, and D. J. Helfand. The FIRST Survey: Faint Images of the Radio Sky at Twenty Centimeters. // 450:559, September 1995.

[54] J. J. Condon, W. D. Cotton, E. W. Greisen, Q. F. Yin, R. A. Perley, G. B. Taylor, and J. J. Broderick. The NRAO VLA Sky Survey. // 115:1693–1716, May 1998.